System 3 from Clontech was used following the manufacturer's instructions. The ABCA1 C terminus region coding for 120 amino acids was cloned from cDNA (13) in pGBKT7. The yeast strain AH109, transformed with pGBKT7/ABCA1-C120, was mated with the yeast strain Y187, which had been pretransformed with a human bone marrow cDNA library. The plasmids, purified from β-galactosidase positive clones, were transformed into *Escherichia coli* and sequenced.

Cellular Lipid Release Assay—Cells were subcultured in poly-L-Lys-coated 6-well plates at a density of 1.0×10^6 cells in Dulbecco's modified Eagle's medium supplemented with 10% (v/v) fetal bovine serum. After 24 h, cells were transfected with ABCA1 and/or FLAG-α1-syntrophin using LipofectAMINE (Invitrogen). After 24 h of incubation, the cells were washed with phosphate-buffered saline (PBS) and incubated in 0.02% bovine serum albumin in Dulbecco's modified Eagle's medium with 10 μg/ml apoA-I. The lipid content in the medium was determined after 24 h incubation as described previously (14).

Immunoprecipitation Analysis—HEK293 cells, transiently expressing ABCA1, were lysed with PBS containing 1% Triton X-100 and protease inhibitors (100 μg/ml 4-(amidino)-phenylmethanesulfonyl fluoride hydrochloride (pAPMSF)), 10 μg/ml leupeptin, and 2 μg/ml aprotinin). Equal amounts of total protein were incubated with 5 μg of anti-FLAG antibody M2 for 1 h at 4 °C. Brain of normal mice and mice lacking α1-syntrophin (α1-*Syn*$^{-/-}$) (12) was homogenized in ice-cold homogenization buffer (10 mM sodium phosphate, 0.4 M NaCl, 5 mM EDTA, pH 7.8, and the protease inhibitors). The particulate fraction was pelleted by centrifugation (12,000 × *g* for 10 min), resuspended in 10 volumes of homogenization buffer, and recentrifuged. Washed pellets were solubilized in homogenization buffer containing 1% Triton X-100 and incubated on ice for 30 min. The suspension was centrifuged again, and the supernatant was then incubated with anti-α1-syntrophin rabbit polyclonal antibody for 100 min at 4 °C. The immunocomplexes were incubated with protein G-Sepharose (Sigma) for 1 h and washed four times with homogenization buffer containing 1% Triton X-100. The bound proteins were separated by SDS-PAGE (7%) and analyzed by immunoblotting using the anti-ABCA1 antibody KM3073 or KM3110.

Immunostaining—HEK293 cells were co-transfected with ABCA1 and FLAG-tagged α1-syntrophin or FLAG-tagged Lin7 using LipofectAMINE. The cells were fixed in 4% paraformaldehyde and 5% sucrose in PBS$^+$ (PBS with 0.87 mM $CaCl_2$ and 0.49 mM $MgCl_2$) for 30 min and permeabilized for 5 min in 0.4% Triton X-100 in PBS$^+$. The cells were blocked with 10% goat serum diluted with PBS$^+$. This was followed by incubation with anti-ABCA1 polyclonal antibody and anti-FLAG M2 antibody. The cells were then stained with Alexa 488-labeled anti-rat IgG antibody and Alexa 564-labeled anti-mouse IgG antibody (Molecular Probes) as secondary antibodies. The fluorescence images were obtained using an Axiovert microscope (Carl Zeiss) equipped with a MicroRadiance confocal laser-scanning microscope (Bio-Rad).

RESULTS

ABCA1 Interacts with Two PDZ-binding Proteins—To search for proteins that are associated with the C-terminal region of ABCA1, a fusion construct of the Gal4 DNA-binding domain with the C-terminal 120 amino acids of human ABCA1 was used as bait for two-hybrid screening. The identified genes contained two PDZ-containing proteins, α1-syntrophin (10 clones) and Lin7 (two clones). To determine whether the interaction between ABCA1 and α1-syntrophin or Lin7 occurs *in vivo*, we transfected FLAG-tagged α1-syntrophin, FLAG-tagged Lin7, or FLAG-tagged vinexin β (15) (as a negative control) together with ABCA1 into HEK293 cells. Lysates prepared from transfected cells were immunoprecipitated with anti-FLAG antibody, and precipitates were evaluated by immunoblotting with anti-ABCA1 antibody. As shown in Fig. 1, ABCA1 was co-immunoprecipitated with FLAG-tagged α1-syntrophin or FLAG-tagged Lin7, but not with FLAG-tagged vinexin β. ABCA1 was not precipitated with mouse IgG control from any of the lysates in which the expression of ABCA1 (Fig. 1) and FLAG-tagged proteins (data not shown) were detected by immunoblotting. More than 25% of the ABCA1 expressed in HEK293 was roughly estimated to be co-immunoprecipitated with FLAG-tagged α1-syntrophin, suggesting strong interaction between ABCA1 and α1-syntrophin (Fig. 2). The interaction between ABCA1 and Lin7 seemed to be weak, because the

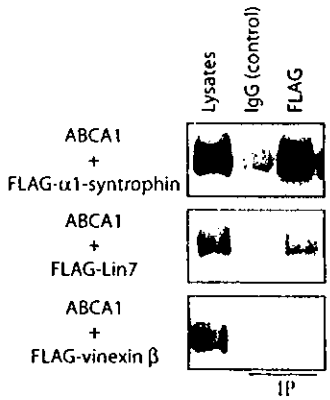

FIG. 1. ***In vivo* association of ABCA1 with α1-syntrophin.** HEK293 cells were co-transfected with human ABCA1 and FLAG-tagged α1-syntrophin, FLAG-tagged Lin7, or FLAG-tagged vinexin β. Cell lysates were immunoprecipitated (*IP*) with anti-FLAG antibody. Immunocomplexes and cell lysates (5%) were subjected to immunoblotting using Anti-ABCA1 monoclonal antibody KM3110, generated against the C-terminal 20 amino acids of ABCA1. Mouse IgG was used as a negative control. The data are representative of three independent experiments.

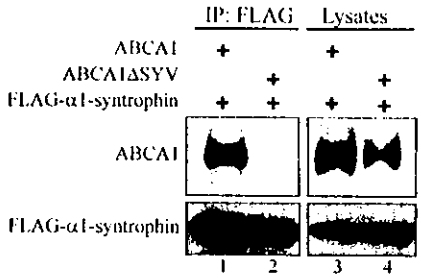

FIG. 2. **ABCA1 interacts with α1-syntrophin via the C-terminal three amino acids.** HEK293 cells were co-transfected with ABCA1 or ABCA1ΔSYV, in which the C-terminal three amino acids were trimmed, and with FLAG-tagged α1-syntrophin. Cell lysates were immunoprecipitated (*IP*) with anti-FLAG antibody. Immunocomplexes and cell lysates (5%) were subjected to immunoblotting using the anti-ABCA1 monoclonal antibody KM3073, generated against the first extracellular domain of the human ABCA1, and an anti-FLAG antibody. The data are representative of two independent experiments.

amount of precipitated ABCA1 with Lin7 was much less than that with α1-syntrophin. The amount of ABCA1 in lysates was consistently higher when co-expressed with α1-syntrophin than with other proteins.

ABCA1 Interacts with α1-Syntrophin via the C-terminal Three Amino Acids—ABCA1 contains the amino acid sequence ESYV at the C terminus, which has been described as a binding target for syntrophin PDZ domains (16). To determine whether the C-terminal three amino acids SYV are important for the interaction, ABCA1ΔSYV, in which these amino acids were trimmed, was co-expressed with FLAG-tagged α1-syntrophin in HEK293 cells. Although the expression of ABCA1ΔSYV was detected in the lysates, no ABCA1ΔSYV was co-precipitated with FLAG-tagged α1-syntrophin. These results suggest that the interaction is mediated with the C-terminal three amino acids SYV of ABCA1 and α1-syntrophin PDZ domains.

Co-localization of the ABCA1 and PDZ-containing Proteins α1-Syntrophin and Lin7—ABCA1 is mainly localized to plasma membrane but is also substantially expressed in intracellular compartments (11, 17–20). To determine whether ABCA1 and α1-syntrophin or Lin7 are co-localized in cells, ABCA1 was co-transfected with FLAG-tagged α1-syntrophin or FLAG-tagged Lin7 into HEK293 cells. The subcellular localization of these proteins was examined under a confocal laser scanning microscope. α1-Syntrophin resided mainly on plasma mem-

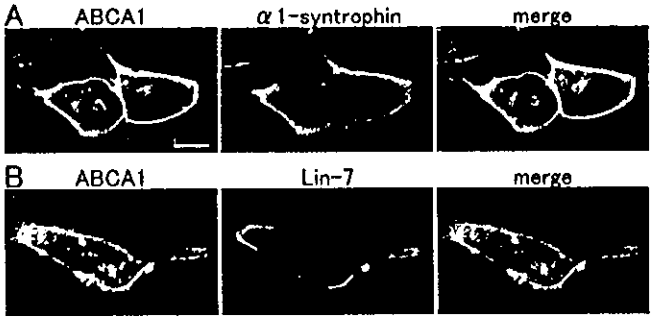

FIG. 3. **Co-localization of ABCA1 and PDZ-containing proteins, α1-syntrophin and Lin7.** HEK293 cells were co-transfected with ABCA1 and FLAG-tagged α1-syntrophin or FLAG-tagged Lin7. The cells were fixed in 4% paraformaldehyde and 5% sucrose, permeabilized in 0.4% Triton X-100, and then doubly stained with anti-ABCA1 polyclonal antibody (*left*) and anti-FLAG antibody (*middle*). A merged image of the staining (*green*, ABCA1; *red*, α1-syntrophin) is also shown (*right*). The data are representative of three independent experiments. *Bar*, 10 μm

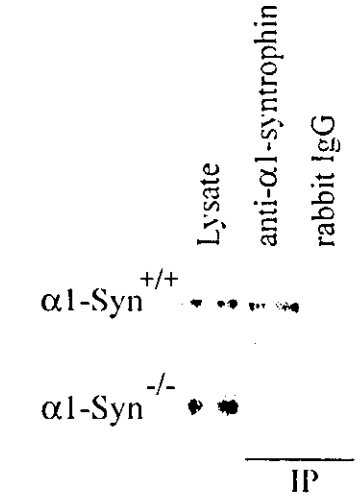

FIG. 4. **Physiological association of mouse ABCA1 with α1-syntrophin.** Brain lysates prepared from normal mouse or α1-syntrophin (−/−) were immunoprecipitated (*IP*) with anti-α1-syntrophin antibody. Immunocomplexes and cell lysates (1%) were subjected to immunoblotting using anti-ABCA1 antibody KM3110. Rabbit IgG was used as a negative control. The data are representative of three independent experiments.

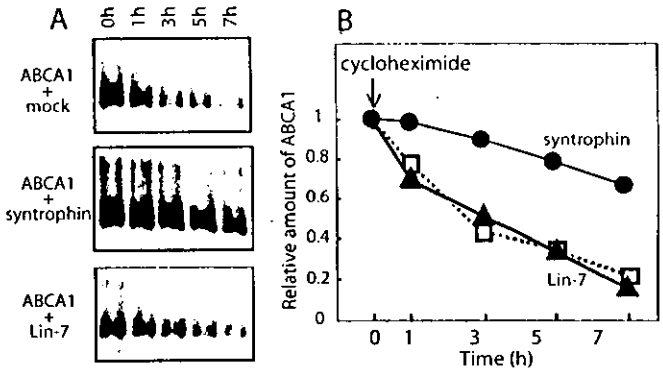

FIG. 5. **α1-Syntrophin modulates turnover of ABCA1.** *A*, HEK293 cells were co-transfected with ABCA1 and vector (*mock*), FLAG-tagged α1-syntrophin, or FLAG-tagged Lin7. At 48 h after transfection, 100 μg/ml of cycloheximide was added to block protein synthesis. After the indicated times, cell lysates were subjected to immunoblotting using Anti-ABCA1 monoclonal antibody KM3110. *B*, quantitation of ABCA1 levels. Values are expressed as fold increase with respect to the amount of ABCA1 just before adding cycloheximide. □, mock transfected; ●, co-transfected with α1-syntrophin; ▲, co-transfected with Lin7. The data are representative of two experiments with similar results.

brane, where it co-localized with ABCA1 (Fig. 3*A*). Lin7 also localized mainly on plasma membrane and appeared not to be uniformly distributed but rather clustered in a specific region of plasma membrane in some cells. In those regions, high expression of ABCA1 and the formation of filopodia were observed (Fig. 3*B*).

Interaction of α1-Syntrophin with ABCA1 in Mouse Brain—Among syntrophin isoforms, α1-syntrophin is mainly expressed in brain, skeletal muscle, and heart in mouse (21). To examine whether ABCA1 and α1-syntrophin interact physiologically, we tried co-immunoprecipitation of these two proteins from mouse brain. Lysates prepared from mouse brain were immunoprecipitated with anti-α1-syntrophin antibody, and precipitates were evaluated by immunoblotting with anti-ABCA1 antibody. As shown in Fig. 4, mouse ABCA1 was co-immunoprecipitated with α1-syntrophin, but not with control IgG. This interaction was confirmed to be specific, because ABCA1 was not precipitated from brain of α1-*Syn*$^{-/-}$ mice (Fig. 4).

α1-Syntrophin Modulates Turnover of ABCA1—Syntrophins have been reported to be involved in protein stability. For example, interaction with β2-syntrophin controls the degradation of ICA512, which connects insulin secretory granules to the utrophin complex and the actin cytoskeleton, by calpain (22), and the stability of AQP4 (23) and neuronal nitric-oxide synthase (12) is suggested as being controlled by α1-syntrophin. The amount of ABCA1 in lysates was consistently higher on co-expression with α1-syntrophin than with other proteins as shown in Fig. 1. Therefore, we examined the effect of α1-syntrophin on the stability of ABCA1. FLAG-tagged α1-syntrophin or FLAG-tagged Lin7 was transiently co-expressed with ABCA1 in HEK293 cells. At 48 h after transfection, the medium was replaced with 10% fetal bovine serum/Dulbecco's modified Eagle's medium containing 100 μg/ml cycloheximide, and cellular protein synthesis was inhibited to block supply of the newly synthesized ABCA1. After the indicated times, the amount of ABCA1 was measured by immunoblotting (Fig. 5*A*). After the inhibition of cellular protein synthesis, 80% of ABCA1 was degraded in 7 h, and the half-life was about 2 h as reported previously (10). Thus, ABCA1 protein turns over rapidly in HEK293 cells. When ABCA1 was co-expressed with α1-syntrophin, only ~30% of ABCA1 was degraded in a 7-h treatment with cycloheximide, and the half-life was estimated to be 10 h (Fig. 5*B*). Lin7, which is a PDZ protein and also binds to the C terminus region of ABCA1, did not show a significant effect on the half-life of ABCA1. The half-life of ABCA1ΔSYV was scarcely affected by co-expression of α1-syntrophin (data not shown). These results suggest that α1-syntrophin decreases ABCA1 protein degradation by interacting with the C terminus three amino acids of ABCA1.

α1-Syntrophin Increases apoA-I-mediated Cholesterol Efflux by ABCA1—To analyze the functional consequences of decreased ABCA1 protein degradation in the presence of α1-syntrophin, the apoA-I-mediated release of cholesterol was examined from HEK293 cells transiently cotransfected with ABCA1 and α1-syntrophin (Fig. 6). Human ABCA1 transiently expressed in HEK293 cells supported the apoA-I-mediated release of cholesterol as previously reported with ABCA1-green fluorescent protein (13). Co-expression of α1-syntrophin significantly increased the apoA-I-mediated release of cholesterol, although expression of α1-syntrophin alone did not affect it.

DISCUSSION

In this study, we identified α1-syntrophin as a protein interacting strongly with ABCA1 via the C-terminal three amino

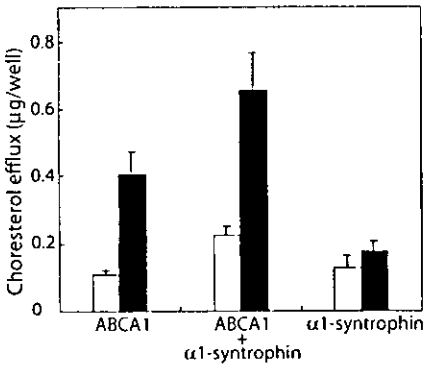

FIG. 6. **Effects of α1-syntrophin co-expression on apoA-I-mediated cholesterol transport.** The cholesterol content of the medium in 6-well plates containing HEK293 cells transiently transfected with ABCA1 alone, ABCA1 and α1-syntrophin, and α1-syntrophin alone was measured after 24 h incubation in the presence (*black bars*) or absence (*white bars*) of 10 μg/ml of apoA-I.

acids SYV of ABCA1. Co-expression of α1-syntrophin retarded degradation of ABCA1 and made the half-life of ABCA1 in HEK293 cells five times longer than in the cells not expressing α1-syntrophin. This effect is not common among PDZ-containing proteins interacting with ABCA1, because Lin7, which also binds to the C terminus region of ABCA1, did not show a similar effect. Co-expression of α1-syntrophin significantly increased the apoA-I-mediated release of cholesterol. Because this interaction was observed in mouse brain, α1-syntrophin could be involved in lipid homeostasis in brain.

Mammalian cells have developed sophisticated mechanisms to ensure adequate cellular cholesterol levels, because cholesterol plays a critical role in several important cell functions, including protein trafficking, membrane vesiculation, and signal transduction, and, at the same time, hyper-accumulation of cholesterol is harmful for cells. Plasma membrane cholesterol content, for example, is regulated through a feedback mechanism controlled by sterol regulatory element binding protein-2 (SREBP-2) (24, 25). To eliminate excess cholesterol from the cell, expression of ABCA1, a key molecule for apoA-I-mediated cholesterol efflux, is stimulated by intracellular oxysterol via the LXR/RXR nuclear receptor (26). The synthesized ABCA1 protein turns over rapidly with a half-life of 1–2 h (8, 10) to cancel cholesterol efflux by ABCA1. Because co-expression of α1-syntrophin retarded degradation of ABCA1 and made the half-life of ABCA1 in HEK293 cells five times longer than in the cells not expressing α1-syntrophin, α1-syntrophin is expected to be involved in intracellular signaling, which determines the stability of ABCA1.

Recently, it has been proposed that ABCA1 is regulated in two different ABCA1 degradation pathways under various cellular conditions: (i) a basal calpain degradation pathway that is turned off by interaction with apolipoproteins (9, 10); and (ii) a ubiquitin-proteasome pathway that is activated by marked free cholesterol loading (27). A sequence rich in proline, glutamate, serine, and threonine (PEST sequence) just before the second membrane spanning domain of ABCA1 (amino acid residue 1283–1306) is involved in regulating the calpain degradation of ABCA1 (10). Although the nature of the apoA-I-ABCA1 interaction is not fully understood, conformational alteration of ABCA1 through the PEST sequence may be induced by its direct or indirect interaction with apoA-I, which may render ABCA1 resistant to proteolysis by calpain. Because ABCA1 was ubiquitinated as well when co-expressed with α1-syntrophin (data not shown), α1-syntrophin seems not to affect ABCA1 degradation in an ubiquitin-proteasome pathway. Binding of α1-syntrophin to the C terminus of ABCA1 may cause a conformational alteration similar to that caused by apoA-I binding and render ABCA1 resistant to proteolysis by calpain.

Syntrophins are a family of five proteins (α1, β1, β2, γ1, and γ2,) containing two pleckstrin homology domains, a PDZ domain, and a C-terminal syntrophin-unique region (28). Analysis of *α-Syn*$^{-/-}$ mouse has demonstrated that perivascular localization of AQP4 in brain requires α1-syntrophin (23) and that the stability of AQP4 (23) and neuronal nitric-oxide synthase (12) decreases in the absence of α1-syntrophin. β2-syntrophin was also reported to interact with ABCA1 and was proposed to participate in the retaining of ABCA1 in cytoplasmic vesicles by forming a ABCA1-β2-syntrophin-utrophin complex (29). It is possible that α1-syntrophin is also involved in endocytotic recycling of ABCA1. Extracellular lipid-free apoA-I may first interact with ABCA1 on plasma membrane, but it is not clear whether the formation of HDL takes place extracellularly or if intracellular events, such as endocytotic recycling, are involved (30). It is intriguing that apoA-I and α1-syntrophin have a similar effect on ABCA1 turnover. A mutation of ABCA1 that causes Tangier disease (W590S) does not affect apoA-I binding or initial ATP binding/hydrolysis but results in a defect in lipid efflux (11, 31, 32). Because apoA-I failed to affect calpain degradation of ABCA1-W590S in HEK293 cells (10), additional signals following apoA-I binding to ABCA1 are speculated to be necessary for the subsequent inhibition of calpain degradation. It is possible that PDZ-containing proteins such as α1-syntrophin are involved in intracellular signaling, which determines the stability of ABCA1.

Acknowledgments—We thank Dr. Shinji Yokoyama for providing lipid-free apoA-I and for helpful discussion. We also thank Dr. Sumiko Abe-Dohmae for technical guidance.

REFERENCES

1. Hara, H., and Yokoyama, S. (1991) *J. Biol. Chem.* **266,** 3080–3086
2. Yokoyama, S. (2000) *Biochim. Biophys. Acta* **1529,** 231–244
3. Francis, G. A., Knopp, R. H., and Oram, J. F. (1995) *J. Clin. Investig.* **96,** 78–87
4. Remaley, A. T., Schumacher, U. K., Stonik, J. A., Farsi, B. D., Nazih, H., and Brewer, H. B., Jr. (1997) *Arterioscler. Thromb. Vasc. Biol.* **17,** 1813–1821
5. Brooks-Wilson, A., Marcil, M., Clee, S., Zhang, L., Roomp, K., van Dam, M., Yu, L., Brewer, C., Collins, J., Molhuizen, H., Loubser, O., Ouelette, B., Fichter, K., Ashbourne-Excoffon, K., Sensen, C., Scherer, S., Mott, S., Denis, M., Martindale, D., Frohlich, J., Morgan, K., Koop, B., Pimstone, S., Kastelein, J., and Hayden, M. (1999) *Nat. Genet.* **22,** 336–345
6. Attie, A. D., Kastelein, J. P., and Hayden, M. R. (2001) *J. Lipid Res.* **42,** 1717–1726
7. Venkateswaran, A., Laffitte, B. A., Joseph, S. B., Mak, P. A., Wilpitz, D. C., Edwards, P. A., and Tontonoz, P. (2000) *Proc. Natl. Acad. Sci. U. S. A.* **97,** 12097–12102
8. Wang, Y., and Oram, J. F. (2002) *J. Biol. Chem.* **277,** 5692–5697
9. Arakawa, R., and Yokoyama, S. (2002) *J. Biol. Chem.* **277,** 22426–22429
10. Wang, N., Chen, W., Linsel-Nitschke, P., Martinez, L. O., Agerholm-Larsen, B., Silver, D. L., and Tall, A. R. (2003) *J. Clin. Investig.* **111,** 99–107
11. Tanaka, A. R., Abe-Dohmae, S., Ohnishi, T., Aoki, R., Morinaga, G., Okuhira, K. I., Ikeda, Y., Kano, F., Matsuo, M., Kioka, N., Amachi, T., Murata, M., Yokoyama, S., and Ueda, K. (2003) *J. Biol. Chem.* **278,** 8815–8819
12. Kameya, S., Miyagoe, Y., Nonaka, I., Ikemoto, T., Endo, M., Hanaoka, K., Nabeshima, Y., and Takeda, S. (1999) *J. Biol. Chem.* **274,** 2193–2200
13. Tanaka, A. R., Ikeda, Y., Abe-Dohmae, S., Arakawa, R., Sadanami, K., Kidera, A., Nakagawa, S., Nagase, T., Aoki, R., Kioka, N., Amachi, T., Yokoyama, S., and Ueda, K. (2001) *Biochem. Biophys. Res. Commun.* **283,** 1019–1025
14. Abe-Dohmae, S., Suzuki, S., Wada, Y., Hiroyuki Aburatani, E. Vance, D., and Yokoyama, S. (2000) *Biochemistry* **39,** 11092–11099
15. Akamatsu, M., Aota, S.-i., Suwa, A., Ueda, K., Amachi, T., Yamada, K. M., Akiyama, S. K., and Kioka, N. (1999) *J. Biol. Chem.* **274,** 35933–35937
16. Gee, S. H., Quenneville, S., Lombardo, C. R., and Chabot, J. (2000) *Biochemistry* **39,** 14638–14646
17. Hamon, Y., Broccardo, C., Chambenoit, O., Luciani, M., Toti, F., Chaslin, S., Freyssinet, J., Devaux, P., McNeish, J., Marguet, D., and Chimini, G. (2000) *Nat. Cell Biol.* **2,** 399–406
18. Fitzgerald, M. L., Mendez, A. J., Moore, K. J., Andersson, L. P., Panjeton, H. A., and Freeman, M. W. (2001) *J. Biol. Chem.* **276,** 15137–15145
19. Remaley, A. T., Stonik, J. A., Demosky, S. J., Neufeld, E. B., Bocharov, A. V., Vishnyakova, T. G., Eggerman, T. L., Patterson, A. P., Duverger, N. J., Santamarina-Fojo, S., and Brewer, H. B., Jr. (2001) *Biochem. Biophys. Res. Commun.* **280,** 818–823
20. Neufeld, E. B., Remaley, A. T., Demosky, S. J., Stonik, J. A., Cooney, A. M., Comly, M., Dwyer, N. K., Zhang, M., Blanchette-Mackie, J., Santamarina-Fojo, S., and Brewer, H. B., Jr. (2001) *J. Biol. Chem.* **276,** 27584–27590
21. Peters, M. F., Adams, M. E., and Froehner, S. C. (1997) *J. Cell Biol.* **138,** 81–93

22. Ort, T., Voronov, S., Guo, J., Zawalich, K., Froehner, S. C., Zawalich, W., and Solimena, M. (2001) *EMBO J.* **20,** 4013–4023
23. Neely, J. D., Amiry-Moghaddam, M., Ottersen, O. P., Froehner, S. C., Agre, P., and Adams, M. E. (2001) *Proc. Natl. Acad. Sci. U. S. A.* **98,** 14108–14113
24. Hua, X., Yokoyama, C., Wu, J., Briggs, M. R., Brown, M. S., Goldstein, J. L., and Wang, X. (1993) *Proc. Natl. Acad. Sci. U. S. A.* **90,** 11603–11607
25. Sato, R., Inoue, J., Kawabe, Y., Kodama, T., Takano, T., and Maeda, M. (1996) *J. Biol. Chem.* **271,** 26461–26464
26. Repa, J. J., and Mangelsdorf, D. J. (2002) *Nat. Med.* **8,** 1243–1248
27. Feng, B., and Tabas, I. (2002) *J. Biol. Chem.* **277,** 43271–43280
28. Kachinsky, A. M., Froehner, S. C., and Milgram, S. L. (1999) *J. Cell Biol.* **145,** 391–402
29. Buechler, C., Boettcher, A., Bared, S. M., Probst, M. C., and Schmitz, G. (2002) *Biochem. Biophys. Res. Commun.* **293,** 759–765
30. Takahashi, Y., and Smith, J. D. (1999) *Proc. Natl. Acad. Sci. U. S. A.* **96,** 11358–11363
31. Fitzgerald, M. L., Morris, A. L., Rhee, J. S., Andersson, L. P., Mendez, A. J., and Freeman, M. W. (2002) *J. Biol. Chem.* **277,** 33178–33187
32. Rigot, V., Hamon, Y., Chambenoit, O., Alibert, M., Duverger, N., and Chimini, G. (2002) *J. Lipid Res.* **43,** 2077–2086

British Journal of Cancer (2004) 91, 1316–1326

www.bjcancer.com

Overexpression of TGF-β by infiltrated granulocytes correlates with the expression of collagen mRNA in pancreatic cancer

Y Aoyagi[1,3], T Oda[1,2,3], T Kinoshita[2], C Nakahashi[2,3], T Hasebe[1], N Ohkohchi[3] and A Ochiai[*,1]

[1]Pathology Division, National Cancer Center Research Institute East, Kashiwanoha 6-5-1, Kashiwa, Chiba 277-8577, Japan; [2]Hepato-Biliary-Pancreatic Surgery Division, National Cancer Center Hospital East, Kashiwanoha 6-5-1, Kashiwa, Chiba 277-8577, Japan; [3]Department of Surgery, Institute of Clinical Medicine, University of Tsukuba, Tennodai 1-1-1, Tsukuba, Ibaraki 305-8575, Japan

Pancreatic cancer is often associated with an intense production of interstitial collagens, known as the desmoplastic reaction. To understand more about desmoplasia in pancreatic cancer, the expression of mRNA for type I and III collagens and potent desmoplastic inducing growth factors transforming growth factor-β (TGF-β), connective tissue growth factor (CTGF), acidic and basic fibroblast growth factor (FGF), platelet-derived growth factor (PDGF) A and C and epidermal growth factor (EGF) was analysed by quantitative RT–PCR. Expression of both collagens in 23 frozen primary pancreatic cancer nodules was significantly higher than that in 15 non-neoplastic pancreatic tissues. The expressions of mRNAs for TGF-β, acidic FGF, basic FGF and PDGF C were likewise higher in surgical cancer nodules, while that of CTGF, PDGF A and EGF were not. Among these growth factors, the expression of TGF-β mRNA showed the most significant correlation with that of collagens ($P<0.0001$). By immunohistochemistry, TGF-β showed faint cytoplasmic staining in cancer cells. In contrast, isolated cells, mainly located on the invasive front surrounding cancerous nests, were prominently and strongly stained. These TGF-β-positive cells contained a segmented nucleus, were negative for anti-macrophage (CD68) and positive for anti-granulocyte antibodies, indicating their granulocytic nature. In conclusion, TGF-β seemed to play a major role among the various growth factors in characteristic overproduction of collagens in pancreatic cancer. Moreover, the predominant cells that express TGF-β were likely to be infiltrated granulocytes (mostly are neutrophils) and not pancreatic cancer cells.
British Journal of Cancer (2004) **91**, 1316–1326. doi:10.1038/sj.bjc.6602141 www.bjcancer.com
Published online 7 September 2004

Keywords: pancreatic cancer; desmoplastic reaction; TGF-β; granulocytes; quantitative RT PCR

Pancreatic adenocarcinoma is a highly lethal disease with no definitive therapy (Warshaw and Fernandez-del Castillo, 1992; Neoptolemos *et al*, 2003). One hallmark of pancreatic adenocarcinoma is the intense production of interstitial components, known as the desmoplastic reaction (Iacobuzio-Donahue *et al*, 2002). As a result, the proportion of pancreatic cancer cells is less than 20–40% of the tumour mass (Kloppel *et al*, 1985), while the remaining 60–80% includes interstitial cells (fibroblast, endocells and inflammatory cells) and proliferated interstitial components include collagens, followed by fibronectin, laminin and proteoglycan (Gress *et al*, 1995; Imamura *et al*, 1995; Linder *et al*, 2001).

The desmoplastic reaction has been reported to be stimulated by various growth factors including epidermal growth factor (EGF) (Gospodarowicz, 1983), platelet-derived growth factor (PDGF) (Gospodarowicz, 1983; Tahara, 1990), connective tissue growth factor (CTGF) (Frazier *et al*, 1996), fibroblast growth factor (FGF) (Gospodarowicz, 1983; Powers *et al*, 2000) and transforming growth factor-β (TGF-β) (Roberts *et al*, 1986; Fine and Goldstein, 1987; Sappino *et al*, 1990; McCartney-Francis and Wahl, 1994). In various malignancies including pancreatic cancer, overexpression of these growth factors is frequently observed (Korc *et al*, 1992; Friess *et al*, 1993; Yamanaka *et al*, 1993; Ebert *et al*, 1995; Gold, 1999; Wenger *et al*, 1999) and has been associated with a significant decrease in the survival and advanced tumour stage (Friess *et al*, 1993). Comprehensive analysis, however, concerning the growth factors that have the strongest impact on the induction of the desmoplastic reaction has never been reported; furthermore, as to which one of the cellular component (i.e. neoplastic cells and interstitial cells) contributing to the overexpression of growth factors inducing desmoplasia in pancreatic cancer has remained obscure. It is generally believed that the cancerous component secretes the growth factors that give rise to this host reaction (Korc *et al*, 1992; Friess *et al*, 1993; Yamanaka *et al*, 1993; Ebert *et al*, 1995; Gold, 1999; Wenger *et al*, 1999). However, as haematopoietic cells including lymphocytes, macrophages and granulocytes are also capable of secreting growth factors (Roberts and Sporn, 1988; Grotendorst *et al*, 1989; Leonardi *et al*, 2000), we hypothesised that infiltrated haematopoietic cells in addition to cancer cell itself could be a source of growth factors that result in induction of desmoplasia.

In order to better understand the molecular mechanism of behind desmoplasia in pancreatic cancer, we have analysed the expression of mRNA of collagens and potent desmoplastic inducing growth factors. We demonstrate that expression of collagens was significantly correlated with that of TGF-β in primary pancreatic cancers, and, moreover, that the main source

*Correspondence: Dr A Ochiai; E-mail: aochiai@east.ncc.go.jp
Received 12 March 2004; revised 14 July 2004; accepted 16 July 2004; published online 7 September 2004

of TGF-β is likely to be infiltrated granulocytes (mostly are neutrophils) and not cancer cells.

MATERIAL AND METHODS

Surgical resected tissues of human pancreatic cancer

The pancreatic cancer tissues used in this study were obtained from patients (10 male; 13 female) undergoing surgery for pancreatic adenocarcinoma in the National Cancer Center Hospital East Japan from 1999 to 2002. The median age was 66 years, ranging from 52 to 81. There was one patient with stage I, two patients with stage II, 10 patients with stage III and 10 patients with stage IV disease. In all, 15 non-neoplastic pancreatic tissues obtained from the same patients were also evaluated. Specimens ranging from 100 to 300 mg were immediately homogenised in TRIZOL reagent solution (Life Technologies, Gaithersburg, MD, USA) using multi-beads shocker (YASUI kikai, Osaka, Japan) after surgical removal. Samples were stored at −80°C until RNA was extracted.

Cultured cell lines

Six human pancreatic cancer cell lines were analysed. ASPC-1, BxPC-3, CAPAN-1 and MiaPaca-2 were obtained from the American Type Culture Collection (ATCC) (Bethesda, MD, USA), PSN-1 was from the Central Animal Laboratory National Cancer Center Research Institute (Tokyo, Japan) and SUIT-2 cells were generously provided by Dr Iwamura (Miyazaki Medical College, Miyazaki, Japan). Two gastric cancer cell lines (KATO3 and MKN45), two colon cancer cell lines (COLO201 and SW1116) and two fibroblast (MRC-5 and WI-38) cell lines were also analysed (ATCC). All cell lines were grown in either RPMI1640 or Dulbecco's modified Eagle medium (Sigma Aldrich, Taufkirchen, Germany) containing 10% heat-inactivated foetal bovine serum (Sigma). All cell lines were kept in a humidified atmosphere containing 5% CO_2 at 37°C. Approximately 1×10^7 cells were sheared in 1 ml of TRIZOL reagent solution using a 21G needle. The homogenate was kept at −80°C until RNA was extracted.

RNA extraction

RNA from surgically resected tissues was extracted from about 100 mg of homogenised tissue in TRIZOL reagent solution. Samples were treated with 40 U of RNase-free DNase I (TAKARA, Shiga, Japan) in 200 μl DEPC (diethylpyrocarbonate)-treated water, 10mM $MgCl_2$ and 40 U of RNase Inhibitor (TOYOBO, Osaka, Japan) at room temperature for 15 min.

Reverse transcription (RT)

All cDNAs were synthesised from 10 μg total RNA using 50 μM oligo $(dT)_{20}$ primer in a total volume of 50 μl using ThermoScript™ RT-PCR System (Life Technologies) according to the manufacturer's protocol. cDNAs were purified using the QIA quick PCR purification Kit (QIAGEN, Hilden, Germany) and eluted in 100 μl of 10 mM Tris-HCl (pH 8.5).

Real-time quantitative RT – polymerase chain reaction (RT – PCR)

Expression of type I collagen and type III collagen mRNAs was analysed since they are major proteins of the stromal component. Transforming growth factor-β, CTGF, acidic FGF (aFGF), basic FGF (bFGF), PDGF A, PDGF C and EGF were analysed as they are potent desmoplastic inducing molecules. Polymerase chain reaction primer pairs for mRNA quantification, intending to flank at least one intron, were designed based on coding sequences obtained from the GenBank Sequence Database (http://www.ncbi.nlm.nih.gov/Genbank/index.html) (Table 1).

Quantitative real-time RT-PCR

Quantitative real-time PCR was carried out using a LightCycler™ instrument (Roche, Mannheim, Germany) using SYBR green. In all, 1 μl of cDNA solution corresponding to 100 ng of total RNA was subjected to 40 PCR cycles of 10 s at 95°C, 10 s at 53 – 65°C and 5 – 15 s at 72°C in a 10 μl mixture containing 1 μl LightCycler-DNA Master SYBR Green I (Roche), 2.25 – 5 mM $MgCl_2$ and 0.25 μM each of forward and reverse gene-specific primers. Polymerase chain reaction conditions and detection temperature of fluorescent products were optimised for each gene by meticulous pilot studies (Table 2). Amplification specificities of the PCR products were confirmed by melting curve analysis of the LightCycler instruments, and re-confirmed by agarose gel electrophoresis.

An external standard curve for each gene was generated using serial 10^2-fold dilutions of RT-PCR products, corresponding to $1 \times 10^8 - 1 \times 10^2$ copies μl^{-1}, to estimate the gene-specific mRNA copy number per 100 ng total RNA of each sample.

Immunohistochemistry

The expression of TGF-β was investigated by immunohistochemistry (IHC) using anti-human TGF-β1 antibody in 23 pancreatic cancer tissues. Potent TGF-β-producing haematopoietic cells, that is, macrophages or granulocytes, were also visualised by IHC. Paraffin-embedded, formalin-fixed sections were subjected to antigen retrieval by immersion in 0.1 M citrate buffer (pH 6.0) and microwaving at 95°C or by incubation with protease K (DAKO, Glostrup, Denmark) at room temperature for 10 min. Endogenous peroxidase was inactivated by incubating in 0.3% H_2O_2 in methanol for 10 – 20 min. Nonspecific binding was blocked by treatment with 5% skim milk and 2% bovine serum albumin in PBS for 30 min. Tissues were then incubated with polyclonal rabbit antibodies against anti-human TGF-β1 (Santa Cruz Biotechnology, Inc., Santa Cruz, CA, USA), as well as

Table 1 PCR primers for collagens and potent desmoplastic inducing growth factors

Gene	Accession no.	Position	Product length (bp)	Forward primer sequence	Reverse primer sequence
Type I collagen	NM_000088	4010–4390	381	5′-CAG TTC GAG TAT GGC GGC G-3′	5′-GAC AGG GCC AAC GTC GAA G-3′
Type III collagen	NM_000090	3637–3936	305	5′-AAA AAG CTG GCG GTT TTG CC-3′	5′-CCG TGG AAC ATT CAA AGG AT-3′
TGF-β	X02812	402–651	250	5′-CTT CAA CAC ATC AGA GCT CCG A-3′	5′-GCC CTC AAT TTC CCC TCC AC-3′
CTGF	M92934	503–871	369	5′-AGC CCA AGG ACC AAA CCG TG-3′	5′-GGC CGT CGG TAC ATA CTC CA-3′
aFGF	X65778	318–468	150	5′-GAA CCA TTA CAA CAC CTA TAT-3′	5′-TTA ATC AGA AGA GAC TGG C-3′
bFGF	M27968	254–445	192	5′-TGA AGG AAG ATG GAA GAT TA-3′	5′-GAA AAA GTA TAG CTT TCT GC-3′
PDGF A	A09204	266–538	273	5′-AGG AAG CTG TCC CCG CTG TC-3′	5′-CGC AGG CGC ACT CCA AAT GC-3′
PDGF C	AF260738	493–739	247	5′-CCA CAA TTC ACA GAA GCT GT-3′	5′-ATC TTA CCT CCT CTG TTA GAA GG-3′
EGF	NM_001963	3246–3586	341	5′-GCC TGC TGA CAC TGA GGA T-3′	5′-CCC TTT GTT GCC ATA ATG GG-3′

Table 2 PCR conditions

Gene	$MgCl_2$ (mM)	Annealing temp. (°C)	Elongation time (s)	Detect temp. (°C)[a]
Type I collagen	2.25	63	15	88
Type III collagen	4	63	10	80
TGF-β	3	65	8	86
CTGF	2.25	66	13	85
aFGF	4	53	5	81
bFGF	5	58	7	72
PDGF A	3	68	10	88
PDGF C	3	56	9	79
EGF	4	65	13	72

[a]Temperature for detection of fluorescent PCR products.

anti-human CD68 mouse monoclonal antibodies (DAKO), and anti-human granulocyte (Medical & Biological Laboratories Co., Nagoya, Japan) at a dilution of 1:100 in a humidified chamber at 4°C overnight. Primary antibody reactions of TGF-β and granulocyte were enhanced using the Envision + kit (DAKO). CD68 antibody treatment was followed by incubation with rabbit anti-mouse secondary antibody and enhanced using Strept AB Complex/HRP kit (DAKO). The immunoreaction was visualised with 0.05% 3,3′-diaminobenzidine (DAB) solution for 1 – 10 min at room temperature. After washing in distilled water, the specimens were counterstained with haematoxylin, dehydrated and mounted.

As negative control for TGF-β1 analysis, the primary antibody was substituted for by anti-green fluorescence protein (GFP) rabbit polyclonal antibodies (Molecular Probes, Inc., Eugene, OR, USA) and processed as described above. As a negative control for granulocyte and macrophage visualisation, anti-mouse H2Kb mouse monoclonal antibodies (PharMingen, San Diego, CA, USA) were used.

Double immunofluorescence stain

In order to corroborate the precise localisation of TGF-β, five representative pancreatic cancer tissues were subjected to double immunofluorescence staining. Sections were incubated with the primary antibody pairs against (TGF-β + CD68) or (TGF-β + granulocyte) for 1 h at room temperature in a humidified chamber. Transforming growth factor-β was labelled red with Alexa Fluor 546 $F(ab')_2$ fragments of goat anti-rabbit IgG (Molecular Probes, Inc., OR, USA) at a dilution of 1:1000, and CD68 and granulocytes were labelled green with fluorescein (FITC) horse anti-mouse IgG (Vector Laboratories, Inc., CA, USA) at a dilution of 1:100 by incubation for 30 min at room temperature. The sections were mounted in PermaFlior™ Aqueous Mounting Medium (ThermoShandon, PA, USA) and examined with a MRC-1024 confocal imaging system (BIO-RAD, Herts, UK).

Statistical analysis

As the expression of mRNAs for type I collagen, type III collagen, TGF-β, CTGF, aFGF, bFGF, PDGF A, PDGF C and EGF exhibited asymmetrical distributions, nonparametric tests (Wilcoxon paired tests) were used. The relationship between expression of collagens and TGF-β, CTGF, aFGF, bFGF, PDGF A, PDGF C and EGF was assessed by linear regression analysis (Mann–Whitney U test). Significance was defined as $P < 0.05$. Statistical calculations were performed with the Stat View software package (Version 5.0: Abacus Concepts, Inc., Berkeley, CA, USA).

Table 3 Expression of collagens and potent desmoplastic inducing growth factors

Gene		Copy number × 10^2 copies/100 ng total RNA	P-value
Type I collagen	C	2497.1 ± 3322.7	0.018
	N	864.6 ± 1087.4	
Type III collagen	C	2103.1 ± 2305.7	0.018
	N	876.0 ± 1143.8	
TGF-β	C	12.9 ± 15.2	0.026
	N	3.8 ± 3.9	
aFGF	C	4.1 ± 5.4	0.002
	N	1.1 ± 2.5	
bFGF	C	4.6 ± 6.5	0.034
	N	1.8 ± 2.2	
PDGF C	C	14.9 ± 23.7	0.028
	N	5.3 ± 11.0	
CTGF	C	212.8 ± 380.3	0.170
	N	96.9 ± 159.7	
PDGF A	C	3.4 ± 3.1	0.347
	N	3.9 ± 5.3	
EGF	C	1.3 ± 3.1	0.179
	N	3.1 ± 5.1	

C = cancerous lesions, N = noncancerous lesions.

RESULTS

Expression of mRNAs for collagens and growth factors in surgical specimens

mRNA copy numbers are listed in Table 3 and represented in Figure 1. In surgically resected pancreatic cancerous lesions (= C), the expression of mRNA for type I collagen and type III collagen was significantly higher (2.9- and 2.4-fold, respectively) compared to non-neoplastic pancreatic tissues (= N) (Table 3, Figure 1A). The expression of mRNA for TGF-β in C was also higher (3.4-fold) than that in N (Figure 1B). The expression of mRNA for aFGF (3.7-fold), bFGF (2.6-fold), PDGF C (2.8-fold) and CTGF (2.2-fold) was also higher in cancer tissue, while that for PDGF A (−1.1-fold) and EGF (−2.5-fold) was lower (Figure 1B). All growth factors with upregulated expression correlated with type I and type III collagen gene expression. (Type I collagen: TGF-β ($r = 0.684$, $P = 0.0003$), CTGF ($r = 0.436$, $P = 0.0376$), aFGF ($r = 0.245$, $P = 0.2591$), bFGF ($r = 0.119$, $P = 0.3206$), PDGF C ($r = 0.562$, $P = 0.0052$), Type III collagen: TGF-β ($r = 0.727$, $P < 0.0001$), CTGF ($r = 0.624$, $P = 0.0015$), aFGF ($r = 0.482$, $P = 0.02$), bFGF ($r = 0.164$, $P = 0.4547$), PDGF C ($r = 0.562$, $P = 0.0007$)). These results indicated that the expression of TGF-β showed high correlation with the expression of type I collagen (Figure 2A) and type III collagen (Figure 2B).

Type I and type III collagen and TGF-β mRNA expression in cell lines

The copy numbers of the collagens and TGF-β mRNA per 100 ng total RNA were analysed for various cell lines. The expression of mRNA for the collagens in fibroblast cell lines was prominent, while the pancreatic cancer cell lines were nearly negative for expression

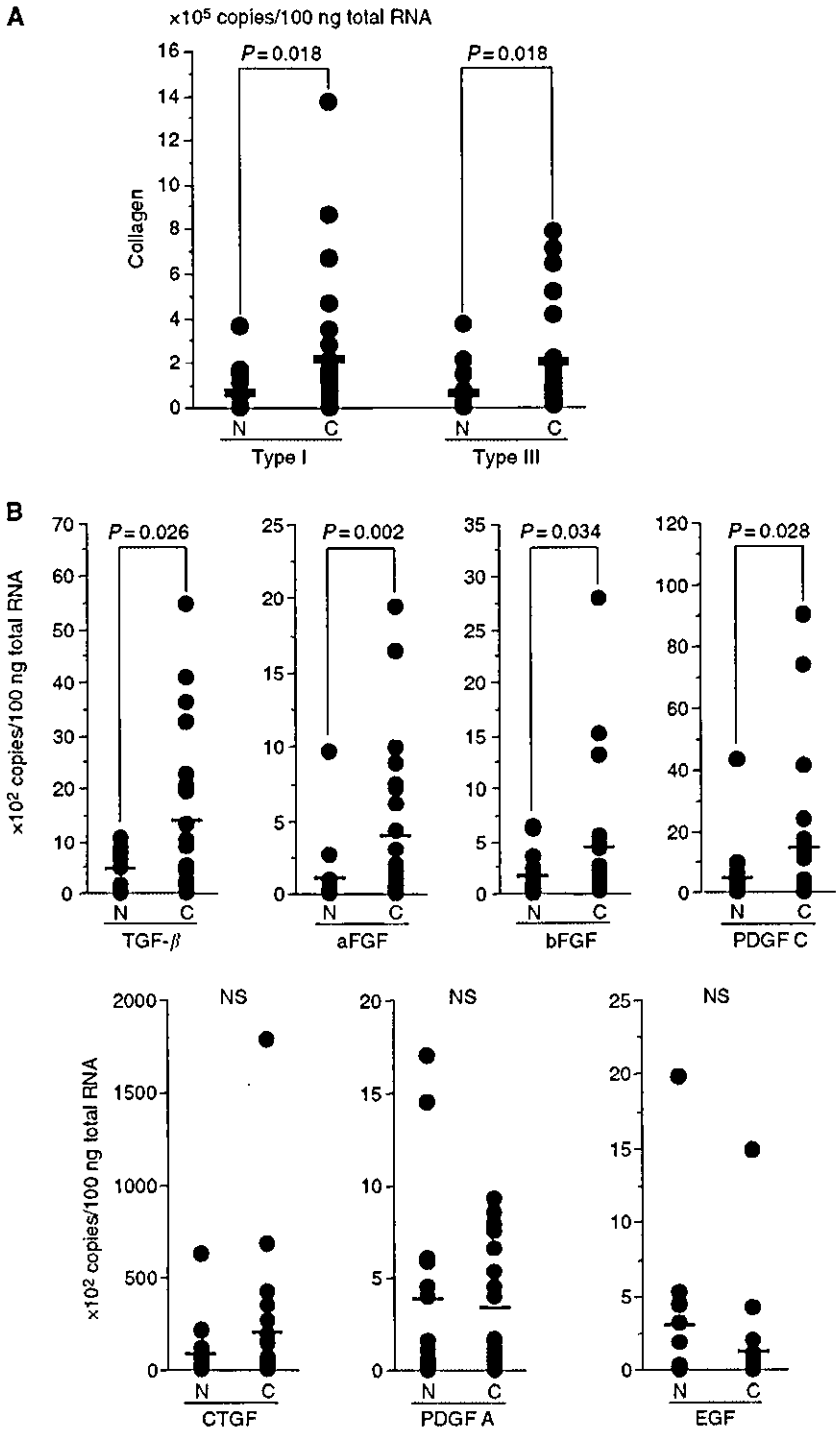

Figure 1 Expressed copy number per 100 ng of total RNA in pancreatic cancerous (C) and noncancerous (N) lesions from surgical specimens as measured by real time RT–PCR. (**A**) Expressions of type I collagen and type III collagen in C were significantly higher than that of N. (**B**) Expressions of TGF-β, aFGF, bFGF and PDGF C in C were significantly higher than that of N, while those of CTGF, PDGF A and EGF were not significant. Bars indicate mean values. NS: not significant.

(Figure 3A). This suggests that fibroblasts may play a crucial role in collagen production, rather than pancreatic cancer cells. Expression of TGF-β is not a specific characteristic of pancreatic cancer cell lines and, in fact, cell lines originating from fibroblasts, gastric cancer and colon cancers also express TGF-β mRNA at the same or higher levels as the pancreatic cancer cell lines (Figure 3B).

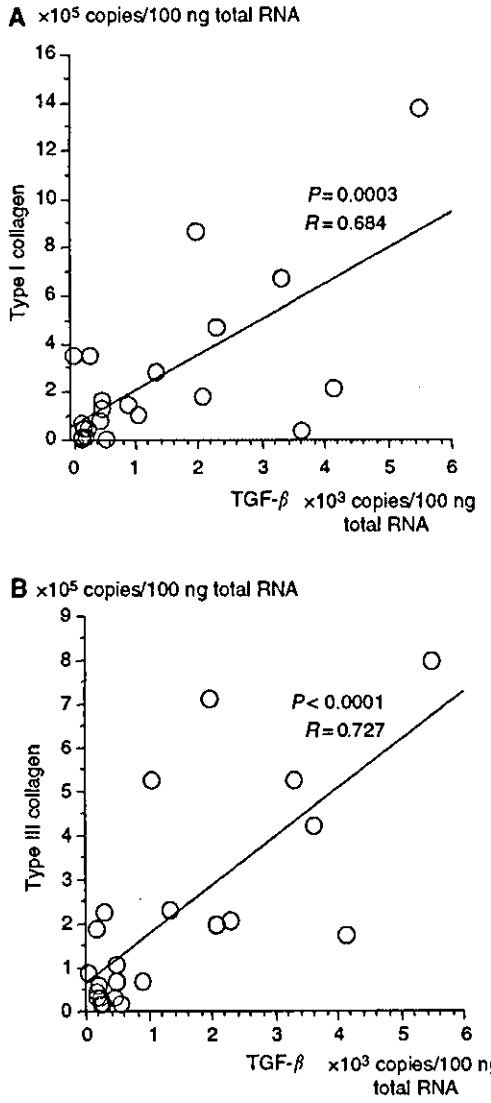

Figure 2 Correlation between TGF-β and type I collagen (**A**), and TGF-β and type III collagen (**B**) mRNA expression in surgical specimens. The expressed copy number of TGF-β and collagens in pancreatic cancer tissues from surgical specimens showed a correlation.

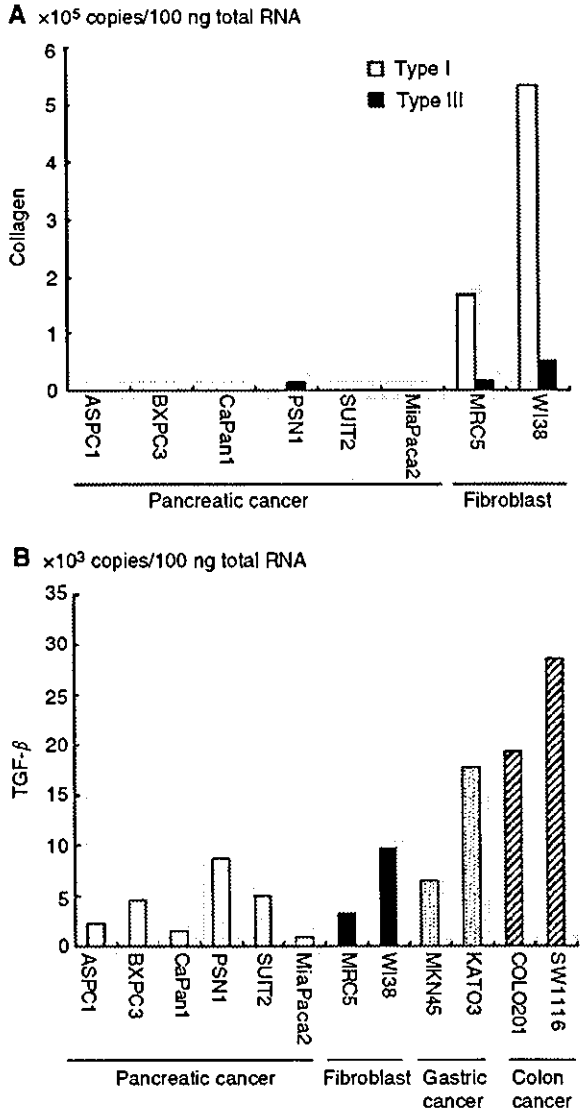

Figure 3 Expression of collagens and TGF-β mRNA in various cancer cell lines. (**A**) Expressions of type I and type III collagens were negative in pancreatic cancer cells, except for a small amount of type III in PSN1 compared with fibroblasts. (**B**) Since the expression of TGF-β in pancreatic cancer cell lines was the same or less than that in fibroblasts, gastric cancer and colon cancer cell lines, it was presumed that TGF-β overexpression is not a specific feature for pancreatic cancer cells.

Immunolocalisation of TGF-β

Since the expression of TGF-β mRNA showed a prominent correlation with the expression of collagen mRNA, the protein distribution of TGF-β in pancreatic cancer tissues was examined using immunohistochemistry. Immunohistochemistry with TGF-β (Figure 4) demonstrated that the staining in pancreatic cancer cells was extremely faint positive at short DAB reaction times (≈1 min) (arrows in Figures 4A and B), and was barely recognisable after longer incubation (≈10 min) (arrows in Figures 4C and D). In contrast, highly prominent immunostaining was observed in isolated cells bordering the cancer nests even at short DAB reaction times (arrow heads in Figures 4A and B). These TGF-β-positive cells were predominantly distributed at the invasive front area (or tumour periphery) (Figures 4A and C), but were rare in the tumour core (Figures 4B and D). High-power field observation of these cells revealed that they possessed bandform and/or segmented nuclei and were presumed to be haematopoietic granulocytes (Figures 4A and C). Immunohistochemistry with anti-GFP rabbit polyclonal antibodies demonstrated complete negative staining for these isolated cells (Figures 4E and F), demonstrating that immunostaining with anti-TGF-β was not an artefact but a result of true immuno-reaction between antigens. The other stromal components such as fibroblasts and endothelial cells showed only weak or no immunostaining (Figure 4).

CD68+ macrophages and antigranulocyte antibody-positive granulocyte cells were also distributed in the area surrounding the cancer nests, similar to the distribution of TGF-β-positive cells

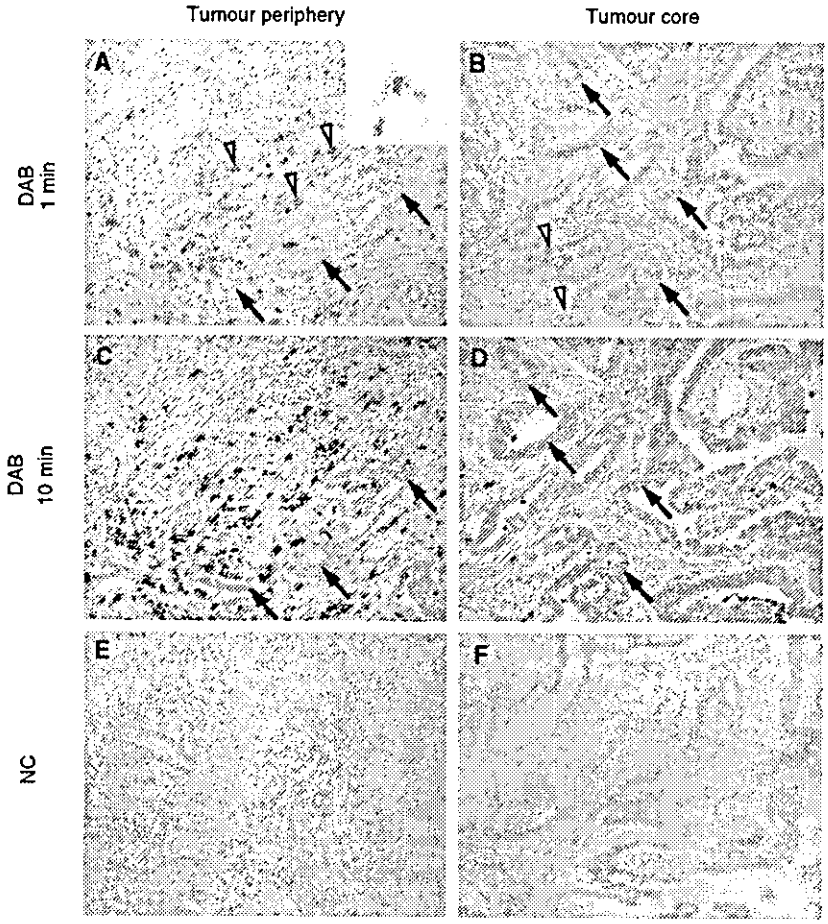

Figure 4 TGF-β immunohistochemistry in pancreatic adenocarcinoma. Transforming growth factor-β immunostaining was visualised by short (≈ 1 min) and long (≈ 10 min) reactions with DAB. Note that staining for cancer cells is barely visible at short DAB staining times (closed arrows) in both the tumour periphery (**A**) and core (**B**), and only slightly apparent after a 10-min reaction (closed arrows) in both the tumour periphery (**C**) and core (**D**). Intense TGF-β immunoreactivity was found in granular cells adjacent to the pancreatic cancer nests, even at short DAB incubation periods (open arrow heads) (**A**, **B**). These TGF-β positive cells were predominantly observed at the tumour periphery (**A**), and are rare in the tumour core (**B**). Immunohistochemistry using anti-GFP rabbit polyclonal antibodies as a negative control against anti-TGF-β rabbit polyclonal antibody resulted in negative staining in both the tumour periphery (**E**) and core (**F**). NC: negative control.

(Figure 5). High-power field observation of these CD68+ macrophages had a single nucleus, while the antigranulocyte antibody-positive granulocyte cells harboured segmented nuclei. Thus, the cells that overexpress TGF-β can be confidently identified as granulocytes. Moreover, in gastric and colon cancer tissues, isolated cells with segmented nuclei around cancer nests at the invasive front also showed strong staining for TGF-β (Figure 6).

Double immunofluorescence stain, (TGF-β + CD68) or (TGF-β + granulocyte)

In order to unambiguously identify the cells producing TGF-β in pancreatic cancer tissues, double immunofluorescence staining was carried out. Distribution of TGF-β-positive cells did not correlate with the distribution of CD68+ cells (Figures 7A–C). However, double staining with anti-TGF-β and antigranulocyte antibodies showed clearly concordant results (Figures 7D–F). These results indicated that the major cellular source of TGF-β in pancreatic tumour tissues, in addition to cancer cells, is granulocytes and not macrophages.

Subtype of granulocytes by morphological observation

In order to identify the subclass of TGF-β-producing granulocytes, careful microscopical observation for haematoxylin–eosin-staining sections was performed. Majorities of the granulocytes were presumed to be neutrophils. As shown in representative pictures in Figures 8A and B, these cells contain polymorphonucleus with cytoplasms stained pink, indicating their neutrophilic feature. Eosinophils, characterised by its distinctive cytoplasmic granules stained red (arrows in Figures 8C and D), were also noted, however, the population of this subtype should at most be 3 – 5% of entire granulocytes.

DISCUSSION

Comprehensive mRNA analysis of several growth factors in pancreatic cancer, including TGF-β, CTGF, aFGF, bFGF, PDGF A, PDGF C and EGF, resulted in the finding that TGF-β is likely to be a potent inducer of the desmoplastic reaction. Furthermore,

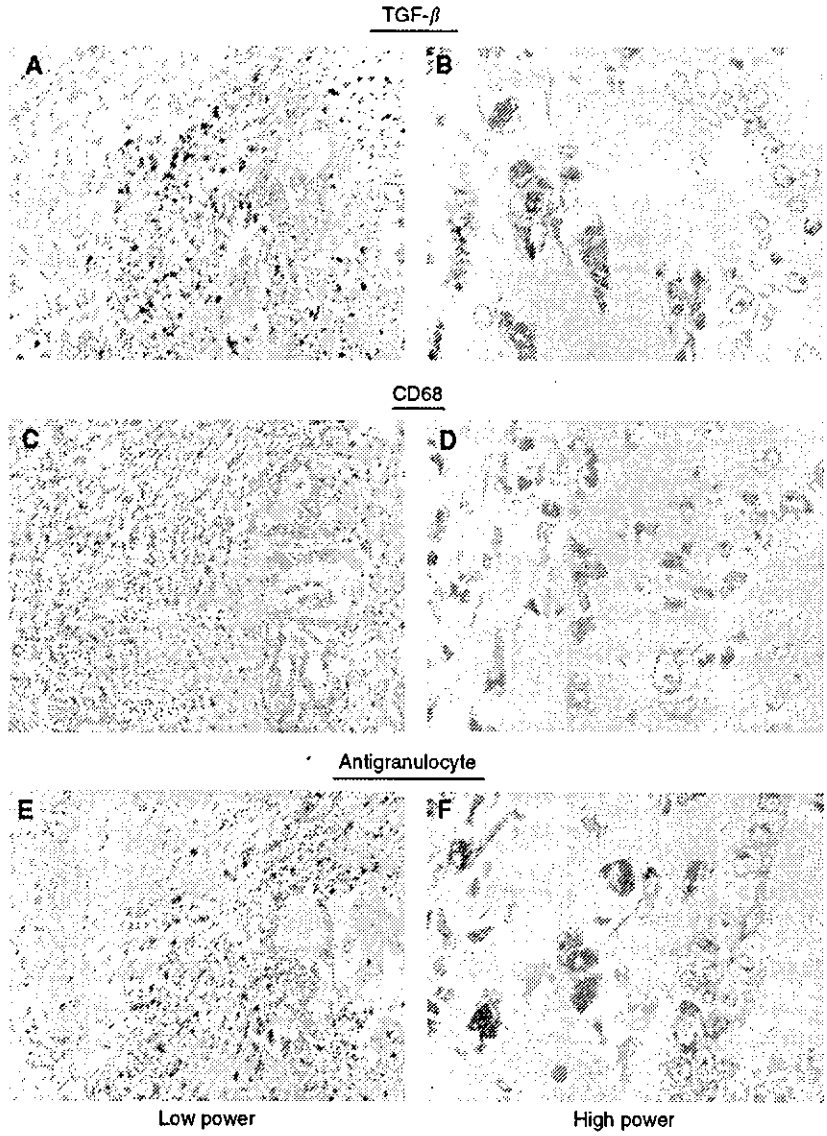

Figure 5 Distribution of TGF-β, CD68 and antigranulocyte-positive cells in pancreatic adenocarcinoma. The distribution of isolated TGF-β-positive cells in pancreatic cancer (**A**) was similar to that of macrophage (i.e. CD68+ cells) (**C**) and granulocytes (**E**) in low power field observation. However, in high power field observation, the morphology of TGF-β1-positive isolated cells (**B**) coincided with antigranulocyte-positive segmented nucleus cells (**F**) but not CD68+ mononuclear cells (**D**).

infiltrated granulocytes (mostly are neutrophils) were highlighted as a predominant source of TGF-β.

In this study, we initially demonstrated that the expression of type I and type III collagens in pancreatic cancer tissues was at least three-fold higher than that in normal pancreatic tissue (Figure 1A), confirming previous reports (Gress *et al*, 1995; Imamura *et al*, 1995; Linder *et al*, 2001). The origin of type I and type III collagens mRNA has been assumed to be cancer stroma (Gress *et al*, 1995), a finding supported by our studies in pancreatic cancer cell lines. Indeed, cancer cells are capable of synthesis and production of extracellular matrix proteins (Niitsu *et al*, 1988; Yoshida *et al*, 1989; Lohr *et al*, 1994), although the expression of collagen mRNAs in the pancreatic cancer cell lines was somewhat lower in comparison to that of fibroblast cell lines (Figure 3A). Furthermore, the expression of collagens from pancreatic cancer cells does not increase *in vivo*, that is, subcutaneous xenotransplantation in immunodeficient mice (unpublished data).

In order to better understand the molecular mechanisms underlying the stromal reaction, we examined the levels of several growth factors capable of inducing desmoplasia. Though plural molecules including TGF-β, aFGF, bFGF and PDGF C were overexpressed in pancreatic cancer (Figure 1B) and presumed to be associated with desmoplasia, we focused on TGF-β since its expression showed the most significant correlation with that of collagens. The expression of TGF-β in pancreatic cancer tissue was actually 3.5-fold higher than that found in normal pancreatic regions (Figure 1B). These results correlate with that of Friess *et al* (1993), who previously reported similar semiquantitative results by Northern blot analysis and/or *in situ* hybridisation. Other authors have reported on the overexpression of TGF-β in various cancer

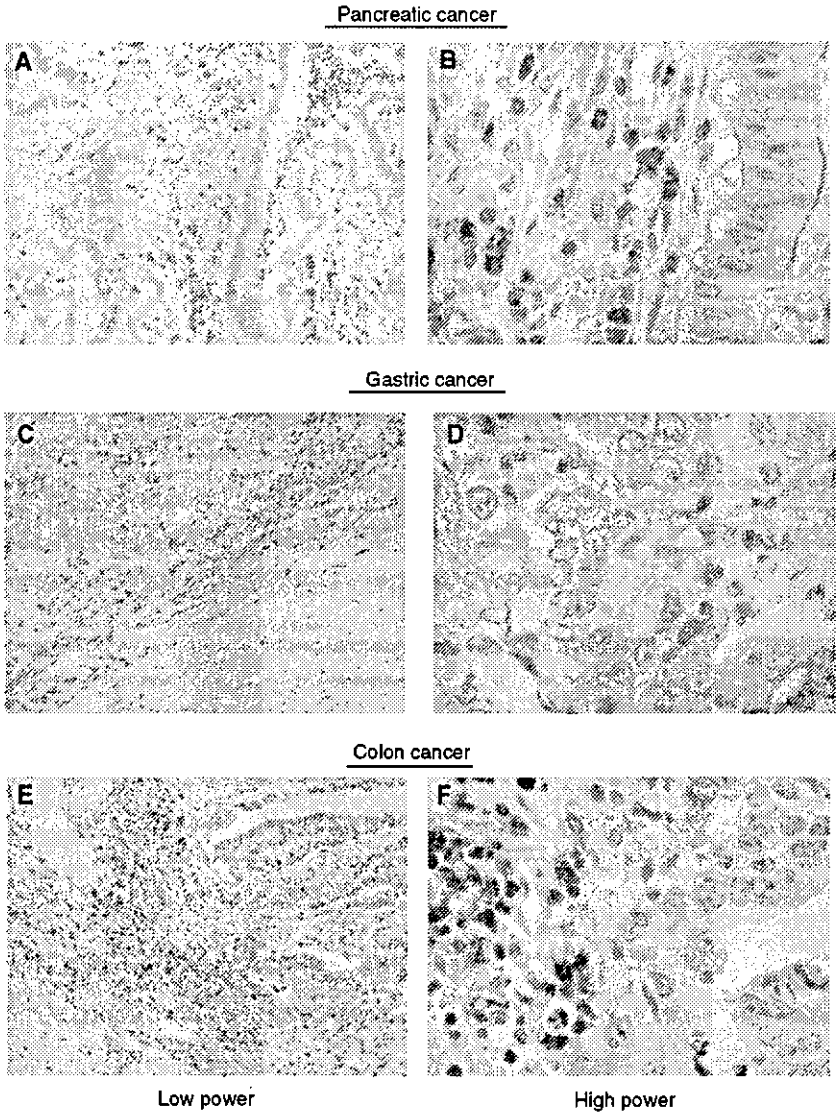

Figure 6 TGF-β immunoreactivity in pancreatic, gastric, and colon cancer tissues. TGF-β immunoreactivity was found in isolated cells around cancer nests in pancreatic cancer tissue (**A**) and many of these cells harboured segmented nuclei (**B**). Transforming growth factor-β-positive segmented nuclei cells were likewise observed in gastric (**C**, **D**) and colon (**E**, **F**) cancers, especially in the tumour periphery. Low power field (**A**, **C**, **E**). High power field (**B**, **D**, **F**).

types by immunohistochemistry, Northern blot analysis and/or *in situ* hybridisation (Samuels *et al*, 1989; Yoshida *et al*, 1989; Barrett-Lee *et al*, 1990; Gorsch *et al*, 1992; Walker and Dearing, 1992; Mahara *et al*, 1994), although none of these methods were quantitative. Our results extend these earlier studies by providing independent, quantitative analysis of the overexpression of TGF-β in pancreatic cancer by employing real-time RT–PCR methods.

While the expressions of both TGF-β and collagens have been examined independently, their expressions relative to one another have not been considered. The utilisation of quantitative RT–PCR method enabled us to evaluate the correlation between the expressions of TGF-β mRNA and collagens. Both *in vitro* and *in vivo* experimental evidence has been accumulating, showing that TGF-β stimulates the production of collagens from fibroblasts. In fact, cultured fibroblasts increased the production of collagen from three- to five-fold when incubated with appropriate concentrations of TGF-β (Raghow *et al*, 1987; Varga *et al*, 1987). When TGF-β was directly injected into the subcutaneous tissue of newborn mice, accelerated fibrosis, that is, activation of fibroblasts to produce collagens, was demonstrated (Roberts *et al*, 1986; Shinozaki *et al*, 1997). In clinical diseases including pulmonary fibrosis and chronic renal allograft damage, TGF-β is also considered to be a main pathogenic factor for the overproduction of collagen (Nicholson *et al*, 1999). Obviously, TGF-β is not the only factor that can stimulate collagen expression in fibroblasts, since insulin and/or growth factors analysed here also regulate the production of type I collagen (Krupsky *et al*, 1996). Nonetheless, it can be stated here that TGF-β may be one of the main inducers of the desmoplastic reaction in pancreatic cancer.

One question concerns the cellular origin of TGF-β in pancreatic cancer nodules. Previous reports have indicated that the upregulated TGF-β originated from cancer cells, since

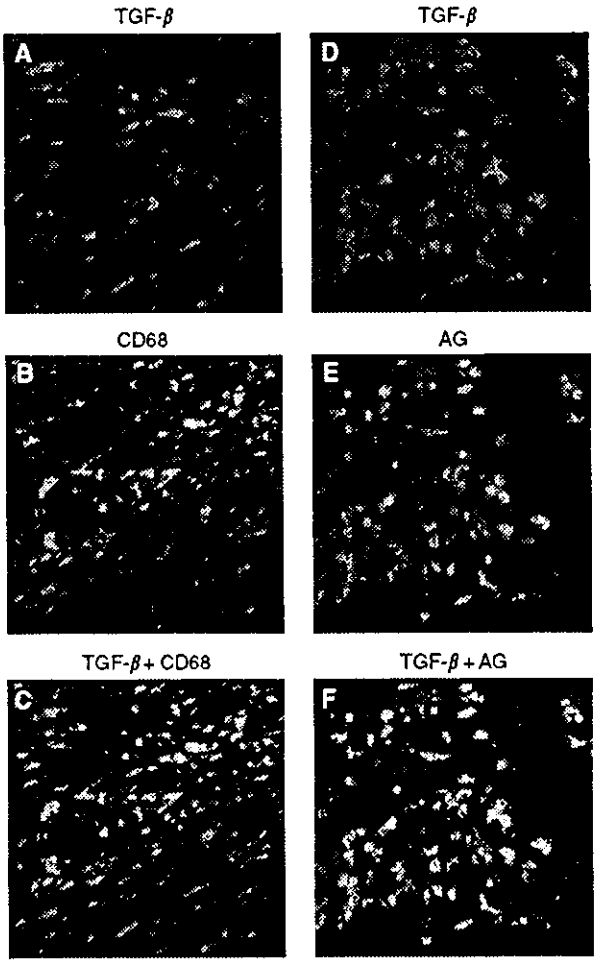

Figure 7 Confocal immunofluorescence images showing TGF-β (red) (**A**, **D**), CD68 as a marker of macrophages (green) (**B**) and granulocytes (green) (**E**). Transforming growth factor-β staining was topographically different from the staining of CD68+ cells (**C**). However, double staining with anti-TGF-β and antigranulocyte antibodies resulted in a consistent overlap (**F**). AG: antigranulocyte.

immunohistochemical and/or *in situ* hybridisation studies demonstrated that the TGF-βs were localised in tumour cytoplasm (Friess *et al*, 1993; Coppola *et al*, 1998). However, it must be considered that the proportion of cancer cells in pancreatic cancer nodules is rather low (20 – 30% at the highest) as a result of desmoplastic reaction (Kloppel *et al*, 1985). If indeed these cancer cells were the origin of overexpressed TGF-β in pancreatic cancer nodules, each cancer cell would be expected to show prominent TGF-β staining. However, our immunohistochemical study for TGF-β demonstrated only faint cytoplasmic staining in cancer cells even after a 10-min reaction with DAB (Figure 4D). In contrast, isolated cells in the surrounding stroma of the cancer nests showed prominent positive staining even after short (1 min) DAB reaction times (Figure 4A). Initially, we assumed that this staining might be due to artefactual staining by endogenous peroxidase. However, staining without incubation of primary antibodies resulted in negative staining for these cells. A second possibility for false-positive staining could also be nonspecific binding of the Fc fragment or trapping of antibody in these isolated cells. In order to rule out this possibility, we carried out incubation with the first antibody with the same type of antibody against an antigen that is not expressed in human tissues, that is, polyclonal rabbit antibody against anti-GFP. Again, this negative control resulted in no staining in these isolated cells (Figures 4E and F). We are therefore confident that the isolated cells in stroma surrounding the cancer nest are actually strongly positive for TGF-β.

It then remained to determine the identity of the cells that overexpress TGF-β. We initially postulated that these cells were macrophages, since it has been reported that macrophages can secrete TGF-β (Assoian *et al*, 1987; Appleton *et al*, 1993) and, moreover, that the expression of TGF-β is associated with fibroblast collagen synthesis (Khalil *et al*, 1989). However, while the distribution of TGF-β-positive cells and CD68+ cells was somewhat similar, double-staining IHC did not show consistent double staining with these two antibodies (Figure 6). We then focused on granulocytes, since these cells, including neutrophils and eosinophils, have also been reported to express TGF-β (Grotendorst *et al*, 1989; Wong *et al*, 1991). Moreover, in the acute phase of disease, neutrophil granulocytes have been shown to express higher amounts of TGF-β mRNA with respect to lymphocytes and monocytes/macrophages (Ossege *et al*, 1996). Furthermore, the TGF-β produced by eosinophils has been shown to be involved in connective tissue remodelling and collagen synthesis (Stahle-Backdahl *et al*, 2000; Nomura *et al*, 2002). As shown in Figure 7, these TGF-β-positive cells coincided extremely well with that of antigranulocyte antibody-positive cells, and morphological evidence supported a notion that majorities of these cells were neutrophils (Figure 8). Together with previous reports that TGF-β is distributed in stromal inflammatory cells including granulocytes as well as cancer cells (Roberts *et al*, 1986; Assoian *et al*, 1987), it seems reasonable to regard that the predominant source of high levels of TGF-β may be infiltrating neutrophil, though bulk tumoral TGF-β should be accumulation of that from neutrophils, eosinophils and cancer cells. A precise and conclusive cellular source of TGF-β in a tumoral context, however, remains to be identified through *in situ* hybridisation.

Neutrophil infiltration is a biological phenomenon that is usually associated with acute inflammation such as bacterial infection. The present pancreatic cancer population was basically free from sign of acute pancreatitis showing high serum amylase level at the time of operation. Furthermore, resected specimens demonstrated no sign of infection such as the presence of pus. We believe that this neutrophil infiltration observed in the present study may be an important phenomenon that should be focused in understanding pancreatic cancer progression. Observation of only the central core of the pancreatic cancer may have missed this neutrophil infiltration, as we demonstrated in Figure 4. In order to evaluate whether infiltration of granulocytes overexpressing TGF-β is specific to pancreatic cancer, we performed immunostaining for TGF-β on gastric and colon cancer samples. As shown in Figure 6, TGF-β-positive granulocytes are clearly present, especially at the invasive front. Thus, TGF-β-secreting infiltrating granulocytes are present in pancreatic, gastric and colon cancer; however, a prominent desmoplastic reaction is observed only in the former. This apparent discrepancy may be explained by the mechanism of activation of TGF-β. Transforming growth factor-β is generally released from cells in a latent, biologically inactive form (Miyazono *et al*, 1993). Following release, it is activated by a variety of mechanisms, including exposure to proteolytic enzymes or alkaline pH conditions (Gleizes *et al*, 1997; Khalil, 1999). The presence of proteases in the pancreas and the alkaline pH of pancreatic juice may result in ideal conditions for activation of latent TGF-β.

In conclusion, we demonstrated that TGF-β is overexpressed in pancreatic cancer nodules and, moreover, that TGF-β is secreted mainly by infiltrating granulocytes (mostly are neutrophils) and not cancer cells. Once secreted, TGF-β can be activated in the unique pancreatic environment, thereby stimulating fibroblasts to

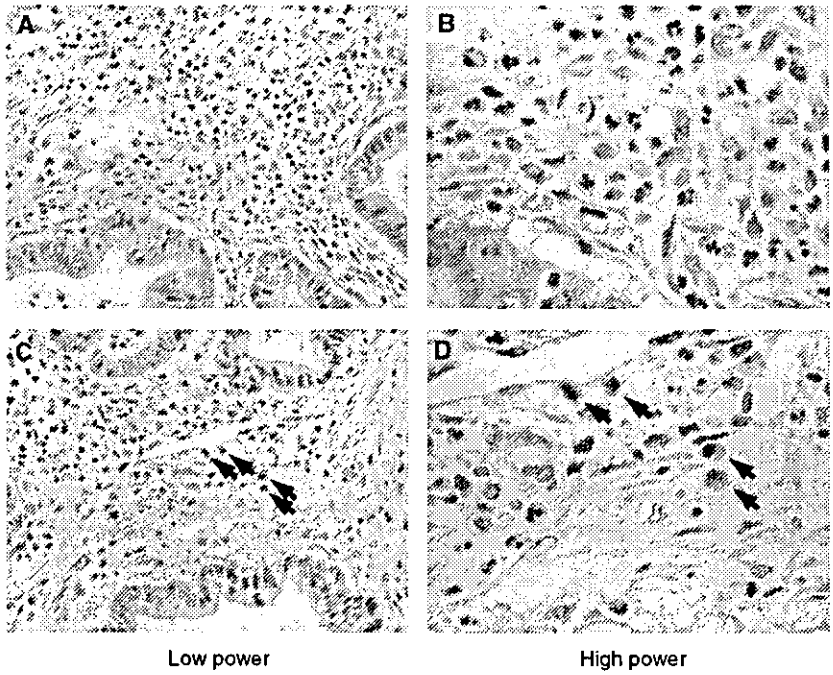

Figure 8 Morphological demonstration of infiltrated granulocytes in pancreatic cancer in Haematoxylin–eosin section. (**A**, **B**) Majorities of isolated cells in stromal, that was the precipitated area of TGF-β-staining positive cells, harboured segmented or polymorpho nuclei with neutrally stained cytoplasmic granules, indicating their neutrophilic nature. (**C**, **D**) Bilobed or trinuclei cells with acidic stained granules (= red), characteristic presentation of eosinophils, are also observed, but the proportion of these cells was at most 3 – 5% of the entire granulocyte. Low power field (**A**, **C**). High power field (**B**, **D**).

produce collagens. In order to interfere with this desmoplastic reaction in pancreatic cancer, a greater understanding and control of the phenomenon of granulocyte infiltration, and control of subsequent activation mechanisms of TGF-β, is urgently required. Furthermore, the meaning of neutrophils infiltration in pancreatic cancer progression, that is, whether it is associated with better or worse prognosis, remains to be elucidated.

ACKNOWLEDGEMENTS

We thank C Okumura and Y Okuhara for their technical assistance. This investigation was supported in part by Cancer Research (11 – 12) from the Ministry of Health and Welfare of Japan, in part by Second Term Comprehensive 10-year Strategy for Cancer Control from the Ministry of Health and Welfare of Japan.

REFERENCES

Appleton I, Tomlinson A, Colville-Nash PR, Willoughby DA (1993) Temporal and spatial immunolocalisation of cytokines in murine chronic granulomatous tissue. Implications for their role in tissue development and repair processes. *Lab Invest* 69: 405–414

Assoian RK, Fleurdelys BE, Stevenson HC, Miller PJ, Madtes DK, Raines EW, Ross R, Sporn MB (1987) Expression and secretion of type beta transforming growth factor by activated human macrophages. *Proc Natl Acad Sci USA* 84: 6020–6024

Barrett-Lee P, Travers M, Luqmani Y, Coombes RC (1990) Transcripts for transforming growth factors in human breast cancer: clinical correlates. *Br J Cancer* 61: 612–617

Coppola D, Lu L, Fruehauf JP, Kyshtoobayeva A, Karl RC, Nicosia SV, Yeatman TJ (1998) Analysis of p53, p21WAF1, and TGF-beta1 in human ductal adenocarcinoma of the pancreas: TGF-beta1 protein expression predicts longer survival. *Am J Clin Pathol* 110: 16–23

Ebert M, Yokoyama M, Friess H, Kobrin MS, Buchler MW, Korc M (1995) Induction of platelet-derived growth factor A and B chains and over-expression of their receptors in human pancreatic cancer. *Int J Cancer* 62: 529–535

Fine A, Goldstein RH (1987) The effect of transforming growth factor-beta on cell proliferation and collagen formation by lung fibroblasts. *J Biol Chem* 262: 3897–3902

Frazier K, Williams S, Kothapalli D, Klapper H, Grotendorst GR (1996) Stimulation of fibroblast cell growth, matrix production, and granulation tissue formation by connective tissue growth factor. *J Invest Dermatol* 107: 404–411

Friess H, Yamanaka Y, Buchler M, Ebert M, Beger HG, Gold LI, Korc M (1993) Enhanced expression of transforming growth factor beta isoforms in pancreatic cancer correlates with decreased survival. *Gastroenterology* 105: 1846–1856

Gleizes PE, Munger JS, Nunes I, Harpel JG, Mazzieri R, Noguera I, Rifkin DB (1997) TGF-beta latency: biological significance and mechanisms of activation. *Stem Cells* 15: 190–197

Gold LI (1999) The role for transforming growth factor-beta (TGF-beta) in human cancer. *Crit Rev Oncog* 10: 303–360

Gorsch SM, Memoli VA, Stukel TA, Gold LI, Arrick BA (1992) Immunohistochemical staining for transforming growth factor beta 1 associates with disease progression in human breast cancer. *Cancer Res* 52: 6949–6952

Gospodarowicz D (1983) Growth factors and their action *in vivo* and *in vitro*. *J Pathol* 141: 201–233

Gress TM, Muller-Pillasch F, Lerch MM, Friess H, Buchler M, Adler G (1995) Expression and *in-situ* localisation of genes coding for extracellular matrix proteins and extracellular matrix degrading proteases in pancreatic cancer. *Int J Cancer* 62: 407–413

Grotendorst GR, Smale G, Pencev D (1989) Production of transforming growth factor beta by human peripheral blood monocytes and neutrophils. *J Cell Physiol* 140: 396–402

Iacobuzio-Donahue CA, Ryu B, Hruban RH, Kern SE (2002) Exploring the host desmoplastic response to pancreatic carcinoma: gene expression of stromal and neoplastic cells at the site of primary invasion. *Am J Pathol* 160: 91–99

Imamura T, Iguchi H, Manabe T, Ohshio G, Yoshimura T, Wang ZH, Suwa H, Ishigami S, Imamura M (1995) Quantitative analysis of collagen and collagen subtypes I, III, and V in human pancreatic cancer, tumour-associated chronic pancreatitis, and alcoholic chronic pancreatitis. *Pancreas* 11: 357–364

Khalil N (1999) TGF-beta: from latent to active. *Microbes Infect* 1: 1255–1263

Khalil N, Bereznay O, Sporn M, Greenberg AH (1989) Macrophage production of transforming growth factor beta and fibroblast collagen synthesis in chronic pulmonary inflammation. *J Exp Med* 170: 727–737

Kloppel G, Lingenthal G, von Bulow M, Kern HF (1985) Histological and fine structural features of pancreatic ductal adenocarcinomas in relation to growth and prognosis: studies in xenografted tumours and clinicohistopathological correlation in a series of 75 cases. *Histopathology* 9: 841–856

Korc M, Chandrasekar B, Yamanaka Y, Friess H, Buchler M, Beger HG (1992) Overexpression of the epidermal growth factor receptor in human pancreatic cancer is associated with concomitant increases in the levels of epidermal growth factor and transforming growth factor alpha. *J Clin Invest* 90: 1352–1360

Krupsky M, Fine A, Kuang PP, Berk JL, Goldstein RH (1996) Regulation of type I collagen production by insulin and transforming growth factor-beta in human lung fibroblasts. *Connect Tissue Res* 34: 53–62

Leonardi A, Brun P, Tavolato M, Abatangelo G, Plebani M, Secchi AG (2000) Growth factors and collagen distribution in vernal keratoconjunctivitis. *Invest Ophthalmol Vis Sci* 41: 4175–4181

Linder S, Castanos-Velez E, von Rosen A, Biberfeld P (2001) Immunohistochemical expression of extracellular matrix proteins and adhesion molecules in pancreatic carcinoma. *Hepatogastroenterology* 48: 1321–1327

Lohr M, Trautmann B, Gottler M, Peters S, Zauner I, Maillet B, Kloppel G (1994) Human ductal adenocarcinomas of the pancreas express extracellular matrix proteins. *Br J Cancer* 69: 144–151

Mahara K, Kato J, Terui T, Takimoto R, Horimoto M, Murakami T, Mogi Y, Watanabe N, Kohgo Y, Niitsu Y (1994) Transforming growth factor beta 1 secreted from scirrhous gastric cancer cells is associated with excess collagen deposition in the tissue. *Br J Cancer* 69: 777–783

McCartney-Francis NL, Wahl SM (1994) Transforming growth factor beta: a matter of life and death. *J Leukoc Biol* 55: 401–409

Miyazono K, Ichijo H, Heldin CH (1993) Transforming growth factor-beta: latent forms, binding proteins and receptors. *Growth Factors* 8: 11–22

Neoptolemos JP, Cunningham D, Friess H, Bassi C, Stocken DD, Tait DM, Dunn JA, Dervenis C, Lacaine F, Hickey H, Raraty MG, Ghaneh P, Buchler MW (2003) Adjuvant therapy in pancreatic cancer: historical and current perspectives. *Ann Oncol* 14: 675–692

Nicholson ML, Bicknell GR, Barker G, Doughman TM, Williams ST, Furness PN (1999) Intragraft expression of transforming growth factor beta1 gene in isolated glomeruli from human renal transplants. *Br J Surg* 86: 1144–1148

Niitsu Y, Ito N, Kohda K, Owada M, Morita K, Sato S, Watanabe N, Kohgo Y, Urushizaki I (1988) Immunohistochemical identification of type I procollagen in tumour cells of scirrhous adenocarcinoma of the stomach. *Br J Cancer* 57: 79–82

Nomura A, Uchida Y, Sakamoto T, Ishii Y, Masuyama K, Morishima Y, Hirano K, Sekizawa K (2002) Increases in collagen type I synthesis in asthma: the role of eosinophils and transforming growth factor-beta. *Clin Exp Allergy* 32: 860–865

Ossege LM, Sindern E, Voss B, Malin JP (1996) Expression of tumour necrosis factor-alpha and transforming growth factor-beta 1 in cerebrospinal fluid cells in meningitis. *J Neurol Sci* 144: 1–13

Powers CJ, McLeskey SW, Wellstein A (2000) Fibroblast growth factors, their receptors and signaling. *Endocr Relat Cancer* 7: 165–197

Raghow R, Postlethwaite AE, Keski-Oja J, Moses HL, Kang AH (1987) Transforming growth factor-beta increases steady state levels of type I procollagen and fibronectin messenger RNAs posttranscriptionally in cultured human dermal fibroblasts. *J Clin Invest* 79: 1285–1288

Roberts AB, Sporn MB (1988) *Advances in Cancer Research* pp 107–145, New York: Academic

Roberts AB, Sporn MB, Assoian RK, Smith JM, Roche NS, Wakefield LM, Heine UI, Liotta LA, Falanga V, Kehrl JH, Fauci AS (1986) Transforming growth factor type beta: rapid induction of fibrosis and angiogenesis *in vivo* and stimulation of collagen formation *in vitro*. *Proc Natl Acad Sci USA* 83: 4167–4171

Samuels V, Barrett JM, Bockman S, Pantazis CG, Allen Jr MB (1989) Immunocytochemical study of transforming growth factor expression in benign and malignant gliomas. *Am J Pathol* 134: 894–902

Sappino AP, Schurch W, Gabbiani G (1990) Differentiation repertoire of fibroblastic cells: expression of cytoskeletal proteins as marker of phenotypic modulations. *Lab Invest* 63: 144–161

Shinozaki M, Kawara S, Hayashi N, Kakinuma T, Igarashi A, Takehara K (1997) Induction of subcutaneous tissue fibrosis in newborn mice by transforming growth factor beta-simultaneous application with basic fibroblast growth factor causes persistent fibrosis. *Biochem Biophys Res Commun* 240: 292–297

Stahle-Backdahl M, Maim J, Veress B, Benoni C, Bruce K, Egesten A (2000) Increased presence of eosinophilic granulocytes expressing transforming growth factor-beta1 in collagenous colitis. *Scand J Gastroenterol* 35: 742–746

Tahara E (1990) Growth factors and oncogenes in human gastrointestinal carcinomas. *J Cancer Res Clin Oncol* 116: 121–131

Varga J, Rosenbloom J, Jimenez SA (1987) Transforming growth factor beta (TGF beta) causes a persistent increase in steady-state amounts of type I and type III collagen and fibronectin mRNAs in normal human dermal fibroblasts. *Biochem J* 247: 597–604

Walker RA, Dearing SJ (1992) Transforming growth factor beta 1 in ductal carcinoma *in situ* and invasive carcinomas of the breast. *Eur J Cancer* 28: 641–644

Warshaw AL, Fernandez-del Castillo C (1992) Pancreatic carcinoma. *N Engl J Med* 326: 455–465

Wenger C, Ellenrieder V, Alber B, Lacher U, Menke A, Hameister H, Wilda M, Iwamura T, Beger HG, Adler G, Gress TM (1999) Expression and differential regulation of connective tissue growth factor in pancreatic cancer cells. *Oncogene* 18: 1073–1080

Wong DT, Elovic A, Matossian K, Nagura N, McBride J, Chou MY, Gordon JR, Rand TH, Galli SJ, Weller PF (1991) Eosinophils from patients with blood eosinophilia express transforming growth factor beta 1. *Blood* 78: 2702–2707

Yamanaka Y, Friess H, Buchler M, Beger HG, Uchida E, Onda M, Kobrin MS, Korc M (1993) Overexpression of acidic and basic fibroblast growth factors in human pancreatic cancer correlates with advanced tumour stage. *Cancer Res* 53: 5289–5296

Yoshida K, Yokozaki H, Niimoto M, Ito H, Ito M, Tahara E (1989) Expression of TGF-beta and procollagen type I and type III in human gastric carcinomas. *Int J Cancer* 44: 394–398

MOLECULAR AND CELLULAR BIOLOGY, Jan. 2005, p. 136–146 Vol. 25, No. 1
0270-7306/05/$08.00+0 doi:10.1128/MCB.25.1.136–146.2005

Cyclic AMP Potentiates Vascular Endothelial Cadherin-Mediated Cell-Cell Contact To Enhance Endothelial Barrier Function through an Epac-Rap1 Signaling Pathway

Shigetomo Fukuhara,[1] Atsuko Sakurai,[1] Hideto Sano,[2] Akiko Yamagishi,[1] Satoshi Somekawa,[1,3] Nobuyuki Takakura,[2] Yoshihiko Saito,[3] Kenji Kangawa,[4] and Naoki Mochizuki[1]*

Department of Structural Analysis[1] and Department of Biochemistry,[4] National Cardiovascular Center Research Institute, Osaka, Department of Stem Cell Biology, Cancer Research Institute, Kanazawa University, Kanazawa,[2] and First Department of Internal Medicine, Nara Medical University, Nara,[3] Japan

Received 2 August 2004/Returned for modification 2 September 2004/Accepted 28 September 2004

Cyclic AMP (cAMP) is a well-known intracellular signaling molecule improving barrier function in vascular endothelial cells. Here, we delineate a novel cAMP-triggered signal that regulates the barrier function. We found that cAMP-elevating reagents, prostacyclin and forskolin, decreased cell permeability and enhanced vascular endothelial (VE) cadherin-dependent cell adhesion. Although the decreased permeability and the increased VE-cadherin-mediated adhesion by prostacyclin and forskolin were insensitive to a specific inhibitor for cAMP-dependent protein kinase, these effects were mimicked by 8-(4-chlorophenylthio)-2′-*O*-methyladenosine-3′, 5′-cyclic monophosphate, a specific activator for Epac, which is a novel cAMP-dependent guanine nucleotide exchange factor for Rap1. Thus, we investigated the effect of Rap1 on permeability and the VE-cadherin-mediated cell adhesion by expressing either constitutive active Rap1 or Rap1GAPII. Activation of Rap1 resulted in a decrease in permeability and enhancement of VE-cadherin-dependent cell adhesion, whereas inactivation of Rap1 had the counter effect. Furthermore, prostacyclin and forskolin induced cortical actin rearrangement in a Rap1-dependent manner. In conclusion, cAMP-Epac-Rap1 signaling promotes decreased cell permeability by enhancing VE-cadherin-mediated adhesion lined by the rearranged cortical actin.

Endothelial cells lining blood vessels regulate endothelial barrier function, which restricts the passage of plasma proteins and circulating cells across the endothelial cells. Endothelial barrier dysfunction results in an increase in vascular permeability, thereby causing edema or inflammatory or metastatic cell infiltration. Inflammatory mediators such as thrombin and histamine induce intercellular gap formation, leading to an increase in endothelial permeability (1, 4). In contrast, angiopoietin 1 and sphingosine-1-phosphate (S1P) stabilize endothelial barrier integrity (17, 18). In addition, cyclic AMP (cAMP), a second messenger downstream of Gs-coupled receptor, improves endothelial cell barrier function (32, 39, 43). Consistently, cAMP-elevating G protein-coupled receptor (GPCR) agonists, adrenomedullin (AM), prostacyclin (PGI2), prostaglandin E2 (PGE2), and β-adrenergic agonists reduce endothelial hyperpermeability induced by inflammatory stimuli (15, 19, 25).

The endothelial cell barrier is structurally organized by adherens junctions (AJ) and tight junctions. Vascular endothelial (VE) cells express both VE-cadherin (also known as cadherin-5 and CD144) and neural (N)-cadherin (9, 33). VE-cadherin constitutes AJ, whereas N-cadherin formed the cell-cell contacts between endothelial cells and endothelial cell-supporting pericytes. VE-cadherin mediates calcium-dependent, homophilic intercellular adhesion. Its short cytoplasmic tail binds to three armadillo family proteins, β-, γ-, and p120-catenins. β- and γ-catenins associated with α-catenin link the VE-cadherin complex to the actin cytoskeleton and, therefore, strengthen the AJ adhesiveness (9).

Endothelial AJ are dynamic structures, and their adhesive property is finely regulated by several different mechanisms. Tyrosine phosphorylation of VE-cadherin, β-catenin, and p120-catenin correlates with weakened endothelial cell-cell adhesion. VE growth factors and inflammatory mediators such as histamine and thrombin induce tyrosine phosphorylation of AJ components, resulting in the weakened cell-cell contacts and increased endothelial cell permeability (1, 14, 40). In clear contrast, angiopoietin 1, which stabilizes cell-cell contacts, induces dephosphorylation of endothelial cell adhesion molecules, VE-cadherin, and platelet endothelial cell adhesion molecule 1 (17). It has been also reported that S1P induces AJ formation and enhances barrier function through a Rac-dependent cortical actin rearrangement (18). cAMP-dependent protein kinase A (PKA) is suggested to be crucial for cAMP-triggered stabilization of cell-cell contacts and for barrier integrity of endothelial cells (43). However, it has not been clear whether PKA-independent signaling is involved in the regulation of endothelial barrier function.

Rap1, belonging to Ras family GTPase, is involved in the formation and stabilization of AJ in *Drosophila melanogaster* (23). Rap1 becomes the GTP-bound active form by guanine

* Corresponding author. Mailing address: Department of Structural Analysis, National Cardiovascular Center Research Institute, 5-7-1 Fujishirodai, Suita, Osaka 565-8565, Japan. Phone: 81-6-6833-5012, ext. 2508. Fax: 81-6-6835-5461. E-mail: nmochizu@ri.ncvc.go.jp.

nucleotide exchange factor (GEF) and the GDP-bound inactive form by GTPase-activating proteins (GAP), respectively. GEFs for Rap1 include C3G, CalDAG-GEFs, Epacs, and DOCK4 (reviewed in reference 6). DOCK4, which is disrupted in various types of human cancers, regulates the formation of AJ (41). Very recent reports also revealed that Rap1 activity is required for the formation of E-cadherin-based cell-cell contacts (20, 36). These findings prompted us to investigate how Rap1 is activated to stabilize cell-cell contacts and to examine the physiological consequence of stabilized cell-cell contacts by Rap1.

In the present study, we investigated the mechanism by which cAMP-elevating GPCR agonists potentiate endothelial barrier function and restrict cell permeability. We found that increased cAMP triggers Epac-Rap1 signaling to reduce permeability independently of PKA by augmentation of VE-cadherin-mediated cell-cell adhesion.

MATERIALS AND METHODS

Reagents and antibodies. Human recombinant AM was kindly provided by Shionogi & Co. Ltd (31). Materials were purchased as follows: isoproterenol (Iso), PGE2, PGI2, thrombin, forskolin (FSK), and 3-isobutyl-1-methylxanthine (IBMX) from Wako Pure Chemical Industries; dibutyryl-cAMP (dbcAMP) from Sigma-Aldrich; H89 from Seikagaku Corporation; 8-(4-chlorophenylthio)-2′-*O*-methyladenosine-3′,5′-cyclic monophosphate (8-CPT-2′-O-Me-cAMP) from Tocris; fluorescein isothiocyanate (FITC)-labeled dextran (molecular weight, 42,000) and purified human immunoglobulin G (IgG) Fc protein from ICN Biologicals; vascular endothelial growth factor (VEGF) from R & D Systems. Anti-Rap1GAPII antibody was developed by immunization of glutathione *S*-transferase (GST)-tagged Rap1GAPII (amino acids 411 to 694 of Rap1GAPII). Other antibodies used here were purchased as follows: anti-VE-cadherin from Chemicon International and Transduction Laboratories; anti-β-catenin from Transduction Laboratories; anti-CREB and anti-phospho-CREB (Ser133) from Cell Signaling Technology; anti-Rap1 from Santa Cruz Biotechnology; anti-cortactin from Upstate Biotechnology, Inc.; rhodamine-phalloidin and Alexa 488-labeled goat anti-mouse IgG from Molecular Probes; horseradish peroxidase-coupled goat anti-mouse and goat anti-rabbit IgG from Amersham Biosciences.

Cell culture and transfection. Human umbilical vein endothelial cells (HUVECs) and human arterial endothelial cells (HAECs) were purchased from Kurabo (Kurashiki, Japan). The cells were maintained in HuMedia-EG2 with a growth additive set as described previously (12) and used for experiments before passages 7 and 10, respectively. HEK293, 293T, and HeLa cells were maintained in Dulbecco's modified Eagle's medium (DMEM; Nissui, Tokyo, Japan) supplemented with 10% fetal bovine serum and antibiotics (100 μg of streptomycin/ml and 100 U of penicillin/ml). HUVECs and 293T cells were transfected by using Lipofectamine Plus reagent (Invitrogen) and by the calcium-phosphate precipitation technique, respectively.

Plasmids and adenovirus. pcDNA-VE-cad-Ect-Fc-His is a modified vector of pcDNA3.1-Fc-PECAM-1 (a kind gift from W. A. Muller, Cornell University) for producing the secreted form of the extracellular domain of VE-cadherin fused with Fc followed by a six-His tag. A DNA fragment encoding human Epac lacking the cAMP binding domain (amino acids 324 to 881) was amplified by PCR with pMT2SM-HA-Epac (a kind gift from J. L. Bos, Utrecht University, Utrecht, The Netherlands) as a template and ligated into the pCXN2 vector (12). pCXN2-FLAG-Rap1V12-IRES-EGFP expressed both FLAG-tagged Rap1V12 and internal ribosomal entry site (IRES)-driven enhanced green fluorescent protein (EGFP), and pCXN2-Rap1GAPII-IRES-EGFP expressed both FLAG-tagged Rap1GAPII and IRES-driven EGFP. pGL3 control vector was purchased from Promega Corp. Recombinant adenoviruses encoding Rap1GAPII (Ad-RapGAP) and LacZ (Ad-LacZ) were obtained from S. Hattori (The Institute of Medical Science, University of Tokyo) and M. Matsuda (Research Institute for Microbial Disease, Osaka University, Osaka, Japan), respectively. Adenoviruses expressing FLAG-tagged Rap1V12 and IRES-driven EGFP (Ad-Flag-Rap1V12-IRES-EGFP) were produced by using the Adeno-X system according to the manufacturer's protocol (Clontech). Endothelial cells were infected with adenoviruses at the appropriate multiplicities of infection (MOI) as described in the figure legends.

Permeability assay. Permeability across the endothelial cell monolayer was measured by using type I collagen-coated transwell units (6.5-mm diameter, 3.0-μm-pore-size polycarbonate filter; Corning Costar Corporation). HUVECs plated at 10^5 cells in each well were cultured for 3 to 4 days before experiments. After serum starvation in medium 199 containing 1% bovine serum albumin (BSA) for 1 h, the cells were treated with the agonists or drugs, as indicated in the figure legends, for 30 min. Permeability was measured by adding 1 mg of FITC-labeled dextran (molecular weight, 42,000)/ml together with or without 2 U of thrombin/ml to the upper chamber. After incubation for 30 min, 50 μl of sample from the lower compartment was diluted with 300 μl of phosphate-buffered saline (PBS) and measured for fluorescence at 520 nm when excited at 492 nm with a spectrophotometer F-4500 (Hitachi). HUVECs infected with adenovirus for 24 h after becoming confluent and kept for another 24 h in replaced medium were subjected to a cell permeability assay.

Immunocytochemistry. Monolayer-cultured HUVECs grown on a 35-mm-diameter glass base dish (Asahi Techno Glass) were starved in medium 199 containing 0.5% BSA for 3 h and subsequently incubated with the stimulants indicated in the figure legends for 30 min. After stimulation, the cells were fixed in PBS containing 2% formaldehyde for 30 min at 4°C, washed with PBS, and permeabilized with 0.05% Triton X-100 for 30 min at 4°C. Cells were blocked with PBS containing 4% BSA for 1 h at room temperature (RT) and stained with rhodamine-phalloidin for 20 min, anti-VE-cadherin for 60 min, and anticortactin for 60 min at RT. Protein reacting with antibody was visualized with Alexa 488-labeled goat anti-mouse IgG. Images were recorded with a confocal microscope (BX50WI, Fluoview; Olympus) with a water immersion objective lens (LUMPlanF1 100X1.00W).

VE-cadherin translocation assay and Western blot analysis. HUVECs plated in six-well plates were serum starved in medium 199 containing 1% BSA overnight. The cells were stimulated with PGI2 and FSK for the indicated time and fractionated with cytoskeleton-stabilizing buffer (10 mM HEPES [pH 7.4], 250 mM sucrose, 150 mM KCl, 1 mM EGTA, 3 mM $MgCl_2$, 1× protease inhibitor cocktail [Roche Diagnostics], 1 mM Na_3VO_4, 0.5% Triton X-100) by centrifugation at 15,000 × *g* for 15 min. The Triton X-100-insoluble fraction was subjected to sodium dodecyl sulfate-polyacrylamide gel electrophoresis (SDS-PAGE) followed by transfer to Immobilon-P (Amersham Biosciences) and immunoblotting with the indicated antibodies. Immunocomplexes were visualized by enhanced chemiluminescence detection (Amersham Biosciences) with species-matched peroxidase-conjugated secondary antibodies.

Purification of recombinant VE-cadherin ectodomain-Fc chimeric protein. 293T cells transfected with pcDNA-VE-cad-Ect-Fc-His were cultured in DMEM supplemented with 10% fetal calf serum for 24 h and subsequently kept in replaced medium (DMEM-F21 containing 1% fetal calf serum) for 7 days. VE-cadherin-Fc (VEC-Fc) protein secreted into the medium was collected every 2 days and centrifuged to remove floating cells and debris. VEC-Fc was collected on ProBond resin (Invitrogen) by gentle agitation overnight at 4°C. VEC-Fc protein bound to the beads was eluted with 500 mM imidazole, concentrated with Amicon Centriplus 30 (Millipore), and buffer exchanged into PBS containing 2 mM $CaCl_2$ and 2 mM $MgCl_2$ (PBS-Ca/Mg) by dialysis.

Cell adhesion assay. Twenty-four-well tissue culture plates were coated with 10 μg of VEC-Fc or Fc protein/ml in PBS-Ca/Mg at 4°C overnight. After washing with PBS-Ca/Mg, the plates were blocked with 1% heat-inactivated BSA in PBS (heat inactivated at 85°C for 12 min) for 1 h at RT. To examine cell adhesion to the VEC-Fc- or Fc-coated dish, cells were suspended in 0.5% BSA-containing medium 199 and incubated for 30 min at 37°C. Cells (1.5×10^5) were plated on each VEC-Fc- or Fc-coated well in the presence or absence of agonists, drugs, and 5 mM EGTA and adhered to the dish at 37°C for the indicated time. To analyze cell adhesion to a collagen-covered surface, cells were plated onto a collagen-coated six-well plate (Iwaki) and adhered to the dish in the presence or absence of 5 mM EGTA. After washing with PBS-Ca/Mg four times to remove nonadherent cells, adherent cells and input cells were quantified by measuring endogenous alkaline phosphatase activity as described elsewhere (35). Briefly, the cells were lysed in a buffer containing 100 mM Tris-citrate (pH 6.5) and 0.25% Triton X-100, and alkaline phosphate activity in the lysate was measured by using the AttoPhos AP fluorescent substrate system (Promega Corp.). To examine the effects of Rap1V12, EpacΔcAMP, and Rap1GAPII, HUVECs were transfected with plasmids encoding either Rap1V12, EpacΔcAMP, or Rap1GAPII together with the luciferase reporter construct (pGL3 control vector). The adhesion of cells expressing Rap1V12, EpacΔcAMP, or Rap1GAPII to the VEC-Fc-coated dish was normalized by measuring the luciferase activity of the cells and input cells (16).

Detection of GTP-bound form of Rap1. Rap1 activity was assessed by a modified Bos's method as described previously (34). Briefly, HUVECs starved in medium 199 containing 1% BSA overnight were stimulated with the indicated

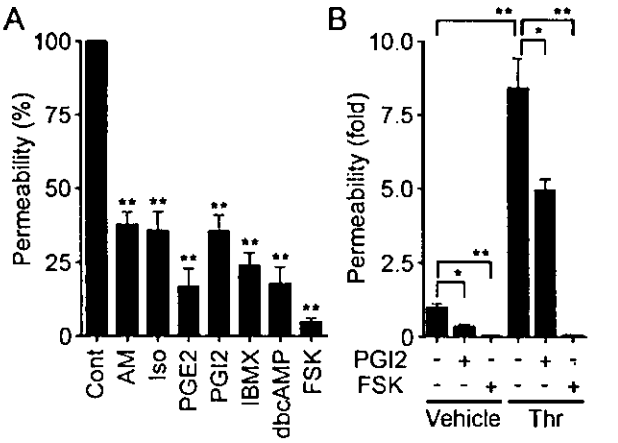

FIG. 1. cAMP enhances barrier function of monolayer VE cells. (A) Vascular permeability, reflecting barrier function, was analyzed by measuring the fluorescence of FITC-labeled dextran across the monolayer-cultured HUVECs as described in Materials and Methods. HUVECs grown on transwell filters were incubated with control (Cont), 0.1 μM AM, 200 μM Iso, 200-ng/ml PGE2, 10-μg/ml PGI2, 1 mM IBMX, 1 mM dbcAMP, and 10 μM FSK for 30 min. Average permeability ± standard deviation is expressed as a percentage compared to the control. (B) The effects of PGI2 and FSK on vascular permeability were quantified in the presence (+) or absence (−) (Vehicle) of 2 U of thrombin (Thr)/ml. Average permeability ± standard deviation is expressed as the increase relative to that observed in unstimulated HUVECs in the vehicle. Data shown are the results from at least three independent experiments. Significant differences from the control (A) or between two groups (B) determined by Student's *t* test are indicated by a single asterisk ($P < 0.05$) or double asterisks ($P < 0.01$).

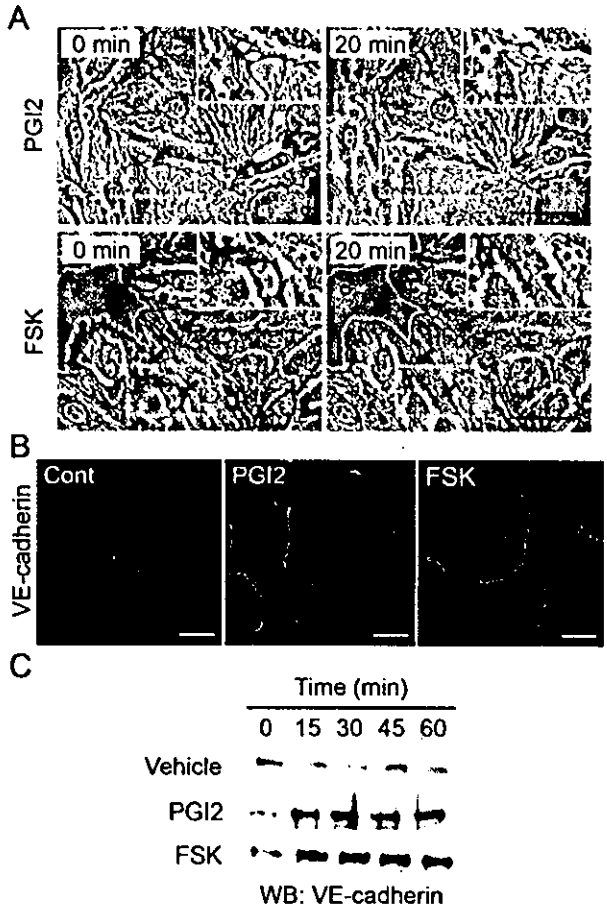

FIG. 2. cAMP induces AJ formation. (A) HUVECs cultured on a glass base dish were stimulated with 10 μg of PGI2/ml (upper panels) or with 10 μM FSK (lower panels) for 20 min and shown as phase-contrast images. Left and right panels show the cells before and after stimulation, respectively. The arrows indicate the sites of cell-cell contacts induced by PGI2 and FSK. The area boxed by the white broken line is enlarged in the right top of the panels. Bars, 50 μm. (B) Subconfluent HUVECs stimulated with vehicle (Cont), 10-μg/ml PGI2, and 10 μM FSK for 45 min were fixed, stained with anti-VE-cadherin antibody, and visualized with Alexa 488-conjugated secondary antibody through a confocal microscope (BX50WI; Olympus). Note that VE-cadherin (green) was accumulated at the cell-cell contact upon PGI2 and FSK stimulation. Bars, 50 μm. (C) Translocation of VE-cadherin was assessed by Triton X-100 solubility. HUVECs were stimulated with vehicle (top), 10-μg/ml PGI2 (middle), and 10 μM FSK (bottom) for the time indicated at the top and fractionated with cytoskeleton-stabilizing buffer as described in Materials and Methods. The Triton X-100-insoluble fraction was subjected to SDS-PAGE followed by Western blot analysis (WB) with anti-VE-cadherin.

agonists and drugs and lysed at 4°C in a pull-down lysis buffer (20 mM Tris-HCl [pH 7.5], 100 mM NaCl, 10 mM $MgCl_2$, 1% Triton X-100, 1 mM EGTA, 1 mM dithiothreitol, 1 mM Na_3VO_4, 1× protease inhibitor cocktail). GTP-bound Rap1 was collected on the GST-Rap1 binding domain of RalGDS precoupled to glutathione-Sepharose beads and subjected to SDS-PAGE followed by immunoblotting with anti-Rap1.

In vivo permeability assay. In vivo permeability was quantified by a modified Miles assay as described previously (29). In brief, ICR mice (Japan SLC, Inc.) shaved 3 days before experiments were lightly anesthetized and intravenously injected with 150 μl of 1% Evans blue dye solution (in saline) passed through a 0.22-μm-pore-size filter. Fifteen minutes later, 20 μl of PBS, VEGF (50 μg/ml), and/or 8-CPT-2′-O-Me-cAMP (1 mM) were applied by intradermal injections with a 30-gauge needle. The sites of intradermal injection were photographed 60 min after the injection, carefully dissected, and weighed. To quantify the vascular permeability, extravasated blue dye was eluted from the dissected skin with formamide at 56°C, and optical density was measured by spectrophotometry at 620 nm.

RESULTS

cAMP enhances the barrier property of monolayer-cultured endothelial cell. To evaluate the barrier function, we examined the permeability of FITC-labeled dextran across monolayer HUVECs. Expectedly, AM, Iso, PGE2, and PGI2 reduced basal endothelial permeability in HUVECs (Fig. 1A). PGI2 also reduced thrombin-induced vascular permeability (Fig. 1B). Other cAMP-elevating bio-ligands similarly reduced thrombin-induced permeability (data not shown). The bio-ligands for cAMP-elevating GPCR that we used in this study indeed increased cAMP in HUVECs (data not shown). Furthermore, IBMX (an inhibitor for phosphodiesterase), dbcAMP (a membrane-permeable cAMP analogue), and FSK (an adenylyl cyclase activator) resulted in a reduction of both basal and thrombin-induced endothelial permeability (Fig. 1; data not shown).

cAMP potentiates formation of AJ. Endothelial barrier function is largely dependent upon endothelial cell junctions. To investigate how cAMP affects AJ formation, we examined AJ organization by immunostaining with anti-VE-cadherin before and after stimulation. When subconfluent HUVECs with intercellular gaps were stimulated with PGI2 or FSK, the cells extended the plasma membrane and established cell-cell contacts with neighboring cells (Fig. 2A). Similar results were

obtained with AM and PGE2 (data not shown). Stimulation of HUVECs with PGI2 and FSK dramatically enhanced accumulation of VE-cadherin at cell-cell contacts (Fig. 2B).

The maturation of AJ requires homophilic binding of intercellular VE-cadherins and tight anchoring to the actin cytoskeleton via the cytoplasmic region through catenins. VE-cadherin anchored to the actin cytoskeleton is detected in detergent-insoluble fractions of cell lysates (26). We found an increase in VE-cadherin in the Triton X-100-insoluble fraction after stimulation with PGI2 or FSK (Fig. 2C). These results suggest that cAMP-elevating GPCR agonists potentiate AJ formation, which results in a cAMP-induced decrease in permeability.

cAMP promotes VE-cadherin-dependent endothelial cell adhesion. VE-cadherin is required for AJ formation (9). To test the involvement of a homophilic interaction of VE-cadherin in cAMP-enhanced AJ formation, we directly examined VE-cadherin-mediated cell adhesion. To mimic the VE-cadherin-dependent cell adhesion, we used VEC-Fc chimeric protein, which consisted of the extracellular domain of VE-cadherin fused to the Fc portion of immunoglobulin. HUVECs were plated onto VEC-Fc-coated dishes and time-lapse imaged. Cells attached within 5 min to the VEC-Fc-coated dish, subsequently spread, and exhibited a typical fried-egg morphology characterized by a large circular lamellipodium (Fig. 3A). No cells attached to the Fc-coated dish (Fig. 3B and C). Since cadherin-dependent cell adhesion requires Ca^{2+}, we examined the effect of Ca^{2+} chelation on cell adhesion to VEC-Fc-coated dishes. Cell adhesion to VEC-Fc-coated dishes was completely abolished by chelating extracellular Ca^{2+}, although cell attachment to the collagen-coated dish was unaffected (Fig. 3C and D). Basal and FSK-augmented cell adhesion to VEC-Fc-coated dishes was inhibited by EGTA (Fig. 3C). Both HUVECs and HAECs expressing VE-cadherin adhered to the VEC-Fc-coated dish (Fig. 3E). In clear contrast, HeLa and HEK293 cells, which express N-cadherin, but not VE-cadherin (20, 42), did not adhere to the VEC-Fc-coated dish, although these cells could attach to the collagen-coated dish (Fig. 3E; data not shown). Collectively, these results indicate that endothelial cell adhesion to the VEC-Fc-coated dish depends upon the homophilic ligation of VE-cadherin.

We proceeded to investigate the effect of cAMP-elevating GPCR agonists on VE-cadherin-mediated cell adhesion. The adhesion of HUVECs plated in the presence of PGI2 or FSK was evaluated by the alkaline phosphatase activity of remaining cells after washing. PGI2 enhanced adhesion of HUVECs to the VEC-Fc-coated dish in a concentration-dependent manner (Fig. 4A) and in a time-dependent manner (Fig. 4B). In a time course analysis, we noticed that enhanced adhesion was observed 7 min after the plating (Fig. 4B). Other cAMP-elevating GPCR agonists, including AM, Iso, and PGE2, potentiated VE-cadherin-dependent cell adhesion (Fig. 4C). In addition, similarly enhanced cell adhesion to the VEC-Fc-coated dish was also observed in the cells treated with cAMP-elevating drugs such as IBMX, dbcAMP, and FSK (Fig. 4F). Like PGI2, the effect of FSK on cell adhesion to the VEC-Fc-coated dish was concentration dependent and time dependent (Fig. 4D and E). This cAMP-induced cell adhesion to the VEC-Fc-coated dish depends on the enhanced homophilic ligation of VE-cadherin because FSK did not augment endothelial adhe-

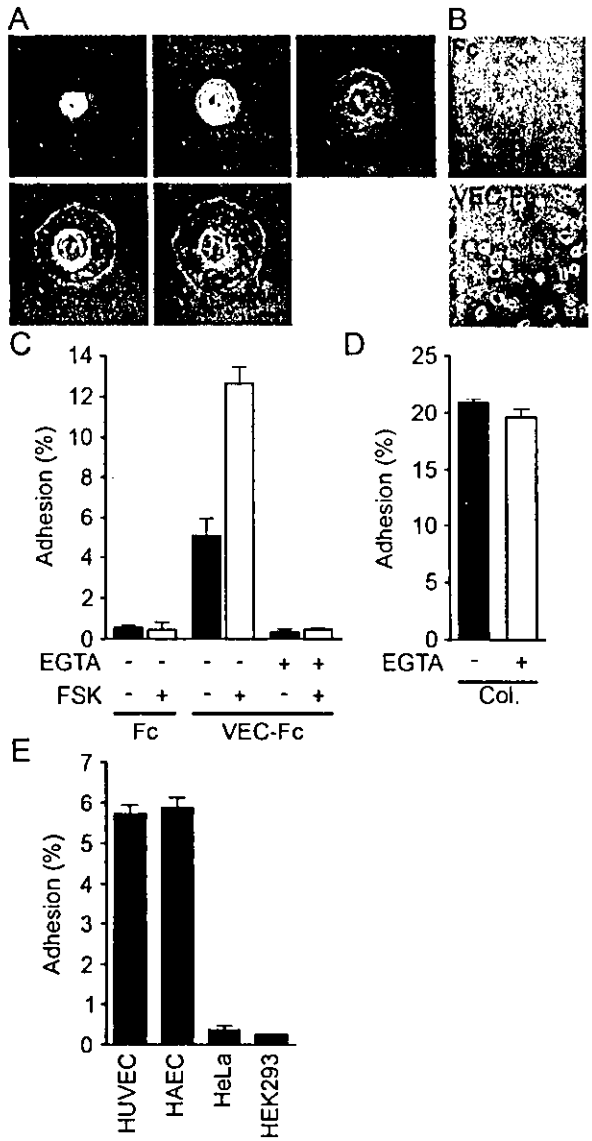

FIG. 3. Endothelial cells adhere to a VEC-Fc-coated dish through homophilic ligation of VE-cadherin. (A) HUVECs were plated onto the VEC-Fc-coated dish and time-lapse imaged at the time points (in minutes) indicated on the panels. Bar, 20 μM. (B) HUVECs were plated on the Fc-coated dish (top panel) or the VEC-Fc-coated dish (bottom panel) for 1 h and phase-contrast imaged after removal of nonadherent cells by washing with PBS-Ca/Mg. (C) HUVECs were plated onto either an Fc- or VEC-Fc-coated dish in the absence (−) or presence (+) of 5 mM EGTA and 10 μM FSK for 7 min. Cell adhesion was quantified as described in Materials and Methods. (D) Adhesion of HUVECs to a collagen-coated dish in the presence or absence of 5 mM EGTA was analyzed by a method similar to that described for panel C. (E) Adhesion of HUVECs, HAECs, and HeLa and HEK293 cells to the VEC-Fc-coated dish was examined as described in the legend for panel C. Cells adhering to the dishes of total input cells (percentage) is expressed as the mean ± standard deviation by measuring alkaline phosphatase activity of adherent cells divided by that of total input cells. Representative results from three independent experiments were shown in all panels.

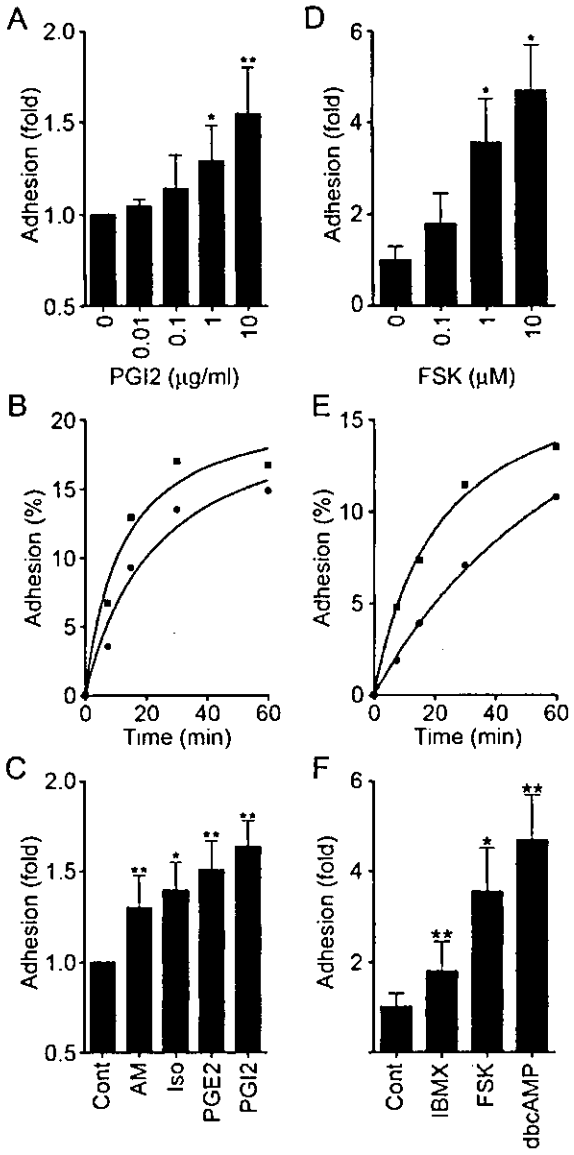

FIG. 4. cAMP potentiates VE-cadherin-dependent cell adhesion. (A) HUVECs were plated onto a VEC-Fc-coated dish in the presence of PGI2 at the concentrations indicated at the bottom for 7 min. Cell adhesion was quantified as described in Materials and Methods. Mean adhesion activity ± standard deviation is expressed as the increase compared with that observed in unstimulated cells. (B) HUVECs were plated onto the VEC-Fc-coated dish in the absence (circle) or presence (square) of 10-μg/ml PGI2 for the time indicated at the bottom. The percent adhesion was calculated by measuring the alkaline phosphatase activity of adherent cells divided by that of total input cells. (C) HUVECs stimulated with cAMP-elevating ligands similar to that described in the legend to panel A were assessed for adhesion activity. The concentration of stimulants was the same as described in the legend to Fig. 1A. (D) The effect of FSK on cell adhesion was analyzed by a method similar to that described for panel A, except that cells were preincubated for 10 min before plating. (E) The effect of 10 μM FSK on time-dependent adhesion was analyzed as described in the legend to panel B, except that cells were preincubated for 10 min before plating. (F) HUVECs stimulated with the reagent indicated at the same concentration used as described in the legend to Fig. 1A were analyzed for cell adhesion by a method similar to that described for panel D. Data are expressed as means ± standard deviations of the results from three independent experiments in panels A, C, D, and F. Representative results from three independent experiments were shown in panels B and E. A significant difference from the control determined by Student's *t* test is indicated with a single asterisk ($P < 0.05$) or double asterisks ($P < 0.01$).

sion to the Fc-coated dish or attachment to the VEC-Fc-coated dish in the absence of extracellular Ca^{2+} (Fig. 3C). These results indicate that cAMP potentiates VE-cadherin-dependent cell adhesion.

cAMP augments endothelial barrier function in a PKA-independent manner. PKA is suggested to be involved in cAMP-enhanced endothelial barrier function (43). Thus, we investigated the involvement of PKA in the regulation of endothelial barrier integrity by PGI2 and FSK. Unexpectedly, PGI2- and FSK-induced reduction of endothelial permeability was insensitive to a specific PKA inhibitor, H89 (7) (Fig. 5A and B). The reduction of thrombin-increased permeability by FSK was also unaffected by H89 (Fig. 5C). Consistently, H89 did not affect VE-cadherin-mediated cell adhesion enhancement by PGI2 and FSK (Fig. 5D and E). To confirm that H89 worked in HUVECs, we examined FSK-induced phosphorylation of CREB, a direct PKA substrate (38). Phosphorylation of CREB upon FSK stimulation was significantly inhibited by H89, indicating the effectiveness of this inhibitor in HUVECs (Fig. 5F). Therefore, these results apparently suggest a novel PKA-independent signaling pathway involved in cAMP-induced endothelial barrier function.

cAMP induces Rap1 activation. Besides PKA, Epac (cAMP-GEF) was identified as a novel cAMP target and a Rap1-specific GEF (5, 21). We therefore hypothesized that cAMP-activated Epac-Rap1 signaling is involved in the enhancement of VE-cadherin-dependent cell adhesion and endothelial barrier function. To address this possibility, we tested whether cAMP-elevating GPCR agonists induce Rap1 activation in HUVECs. Rap1 activity was determined by a pull-down assay by using a GST fusion protein of Rap1-binding domain of RalGDS according to the Bos's method. Bio-ligands for cAMP-elevating GPCR activated Rap1 (Fig. 6A). PGI2 rapidly induced Rap1 activation, which peaked at 1 to 5 min after the stimulation and then declined to the basal level by 10 min (Fig. 6C). A second wave of Rap1 activation was also observed 15 to 45 min after the stimulation (Fig. 6C). PGI2-induced Rap1 activation occurred in a concentration-dependent manner (Fig. 6B), which was associated with enhancement of VE-cadherin-dependent cell adhesion (Fig. 4A). Similarly, dbcAMP, FSK, and IBMX activated Rap1 (Fig. 6D). FSK-induced Rap1 activation reached a maximal level 2 to 5 min after the stimulation, and the level was sustained for up to 15 to 30 min (Fig. 6E). Collectively, these findings indicate that cAMP induces Rap1 activation in endothelial cells.

Specific activation of Epac reduces endothelial permeability and enhances VE-cadherin-dependent cell adhesion. To test whether the activation of endogenous Epac is sufficient to reduce endothelial permeability and to induce VE-cadherin-dependent cell adhesion, we used a recently developed cAMP analog, 8-CPT-2′-O-Me-cAMP, which specifically activates Epac without affecting PKA activity (13). As expected, 8-CPT-2′-O-Me-cAMP induced Rap1 activation in HUVECs (Fig. 7A), indicating that Epac is expressed in endothelial cells.